BRNO UNIVERSITY OF TECHNOLOGY
VYSOKÉ UČENÍ TECHNICKÉ V BRNĚ

FACULTY OF CIVIL ENGINEERING
ÚSTAV STAVEBNÍ MECHANIKY

FAKULTA STAVEBNÍ
INSTITUTE OF STRUCTURAL MECHANICS

TENSILE STRENGTH OF FIBROUS YARNS AND COMPOSITES

DOCTORAL THESIS
DIZERTAČNI PRÁCE

AUTHOR
AUTOR PRÁCE

ROSTISLAV RYPL

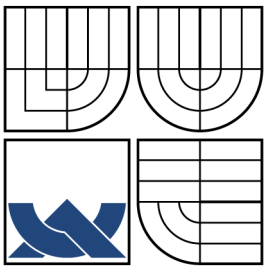

BRNO UNIVERSITY OF TECHNOLOGY
VYSOKÉ UČENÍ TECHNICKÉ V BRNĚ

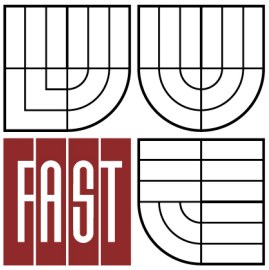

FACULTY OF CIVIL ENGINEERING
ÚSTAV STAVEBNÍ MECHANIKY

FAKULTA STAVEBNÍ
INSTITUTE OF STRUCTURAL MECHANICS

TENSILE STRENGTH OF FIBROUS YARNS AND COMPOSITES

TAHOVÁ PEVNOST VLÁKNITÝCH SVAZKŮ A KOMPOZITŮ

DOCTORAL THESIS
DIZERTAČNI PRÁCE

AUTHOR
AUTOR PRÁCE
ROSTISLAV RYPL

SUPERVISOR
VEDOUCÍ PRÁCE
prof. Ing. MIROSLAV VOŘECHOVSKÝ, Ph.D.

BRNO 2015

ABSTRACT

Technical textiles play a highly important role in today's material engineering. In fibrous composites, which are being applied in a number of industrial branches ranging from aviation to civil engineering, technical textiles are used as the reinforcing or toughening constituent. With growing number of production facilities for fibrous materials, the need for standardized and reproducible quality control procedures becomes urgent.

The present thesis addresses the issue of tensile strength of high-modulus multifilament yarns both from the theoretical and experimental point of view. In both these aspects, novel approaches are introduced. Regarding the theoretical strength of fibrous yarns, a model for the length dependent tensile strength is formulated, which distinguishes three asymptotes of the mean strength size effect curve. The transition between the model of independent parallel fibers applicable for smaller gauge lengths and the chain-of-bundles model applicable for longer gauge lengths is emphasized in particular. It is found that the transition depends on the stress transfer or anchorage length of filaments and can be identified experimentally by means of standard tensile tests at different gauge lengths.

In the experimental part of the thesis, the issue of stress concentration in the clamping has been addressed. High-modulus yarns with brittle filaments are very sensitive to stress concentrations when loaded in tension making the use of traditional tensile test methods difficult. A novel clamp adapter for the Statimat 4U yarn tensile test machine (producer: Textechno GmbH) has been developed and a prototype has been built. A test series comparing yarns strengths tested with the clamp adapter and with commonly used test methods has been performed and the results are discussed. Furthermore, they are compared with theoretical values using the Daniels' statistical fiber-bundle model.

KEYWORDS

fibrous yarns; probability and statistics, size-effect, tesile test of fibrous yarns

ABSTRAKT

Technické textilie hrají v současnosti velmi důležitou roli v materiálovém inženýrství. Používají se pro vyztužování nebo zvyšování houževnatosti ve vláknitých kompozitech, které nachází uplatnění v celé řadě průmyslových odvětví sahajících od aeronautiky až po stavební inženýrství. S rostoucí produkcí vláknitých materiálů roste také potřeba standardizovaných a reprodukovatelných metod řízení jakosti.

Tato doktorská práce se zaměřuje na tahovou pevnost vysokomodulových vláknitých svazků z teoretického i praktického úhlu pohledu. V obou těchto aspektech jsou představeny nové přístupy. Co se týče teoretické pevnosti vláknitých svazků, je v této práci formulován model délkově závislé tahové pevnosti, který rozlišuje tři asymptotická chování pevnosti v závislosti na délce. Zdůrazněna je především problematika přechodu z módu svazku nezávislých paralelních vláken (kratší svazky) do módu řetězce nezávislých svazků (delší svazky). Ukazuje se, že tento přechod závisí na kotevní délce vláken ve svazku a je možné jej experimentálně identifikovat pomocí standardních tahových zkoušek svazků na různých délkách.

V experimentální části práce se autor zabývá koncentrací napětí v uchycení svazků při tahové zkoušce. Vysokomodulové svazky s křehkými vlákny jsou v průběhu tahové zkoušky velmi náchylné ke koncentracím napětí, což často znemožňuje použití standardních metod pro jejich zkoušení. V rámci této práce byl vyvinut a vyroben adaptér uchycení pro existující zkušební stroj Statimat 4U firmy Textechno GmbH. Byla provedena série komparativních tahových zkoušek na vláknitých svazcích s vyvinutým adaptérem a standardními metodami a výsledky jsou v práci diskutovány. Tyto zkoušky jsou rovněž porovnány s teoretickou pevností svazků predikovanou Danielsovým statistickým modelem pro svazky.

KLÍČOVÁ SLOVA

vláknité svazky, pravděpodobnost a statistika, vliv velikosti, tahová zkouška vláknitých svazků

RYPL, Rostislav *Tensile strength of fibrous yarns and composites*: doctoral thesis. Brno: Brno University of Technology, Faculty of Civil Engineering, Ústav stavební mechaniky, 2015. 75 p. Supervised by prof. Ing. Miroslav Vořechovský, Ph.D.

Prohlášení:

Prohlašuji, že jsem doktorskou práci zpracoval(a) samostatně a že jsem uvedl(a) všechny použité informační zdroje.

Brno ....

(podpis autora)

Acknowledgement:

Rád bych poděkoval vedoucímu doktorské práce panu prof. Ing. Miroslavu Vořechovskému, Ph.D. za odborné vedení, konzultace a podnětné návrhy k práci. Dále bych rád poděkoval za finanční podporu Grantové agentuře ČR v rámci projektu GC13-19416J a MŠMT v rámci projektu FAST-S-13-1889.

CONTENTS

LIST OF FIGURES

LIST OF TABLES

1 INTRODUCTION

1.1 Motivation

The 20th century has witnessed an uprise of fibrous composites. Fibrous reinforcement has been used both for reinforcing polymer and metal matrices and toughening ceramic matrices. As the production of high modulus and high strength fibers – made of both ceramic and polymer materials – has grown in efficiency and thus has become more economic, the supreme properties of fibrous composites have been exploited by an ever wider range of industry branches. Having been discovered for aviation and sport, the domain of fibrous composites expanded over energy and automotive and, finally has reached civil engineering, where the strength and stiffness to weight and price ratio became interesting only at the end of the 1990s. There are in general three fundamental parts determining the mechanical behavior of fibrous composites:

1) fibers (reinforcing or toughening)
2) matrix (polymer, ceramic, metal)
3) interface between fibers and matrix

Even though there have been endless discussions on the hierarchy of priorities of these three components, it is probably most apt to conclude that each one plays a significant role with none of them being less important than the others.

For the most part, this thesis thoroughly examines the fibrous constituent separately. The understanding of the complex behavior of the fibrous constituent alone – fibers, bundles and yarns – provides much inside into the composite behavior and is of great significance for simulating the composite mechanics. However, in the last chapter, the interaction of short fiber bundles with cement-based matrix and the resulting composite called glass fiber reinforced concrete (GFRC) are analyzed.

Being a brittle material whose strength is governed by the weakest link, high-modulus fibers and fiber bundles exhibit various size-effects, which are in their elementary tendencies depicted in Fig. 1.1. On one hand, the tensile strength decreases with the gauge length of the fibrous material. On the other hand, the strength de-

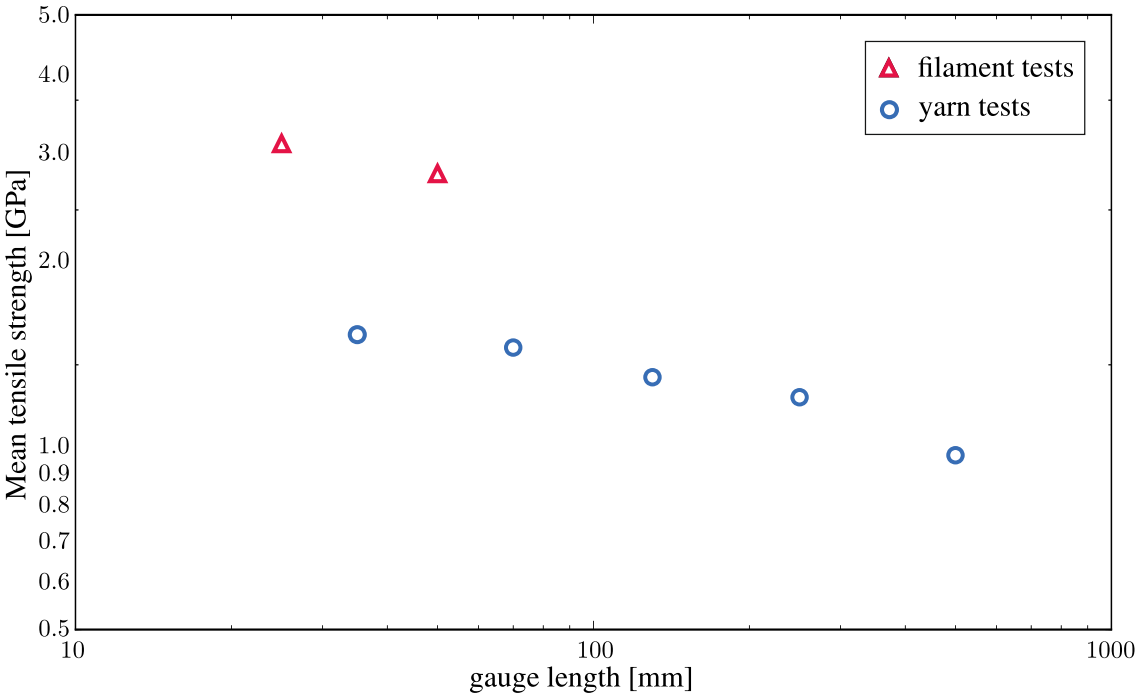

Fig. 1.1: Demonstration of size-effect in the tensile strength of high-modulus fibrous material: log-log plot of carbon filament and carbon yarn tensile strengths at various gauge lengths.

creases with the number of fibers in the bundle. In particular, the strength of a single fiber is on average about 20% higher than the strength of a multi-filament yarn. As shall be revealed in the body of the thesis, this tendency only applies for a range on gauge lengths and is violated above a transition threshold. Clearly, the tensile strength of fibrous materials is not a trivial quantity to identify and a number of mechanisms have to be understood in order to predict the tensile strength in a range extrapolated beyond experimentally measured data.

1.2 Goal setting

The main goals of this work can be summarized as follows:

(1) Provide a probabilistic model of the strength of high-modulus fibrous material for the complete range of gauge lengths.

(2) Address the clamping issue in tensile testing of fibrous yarns and propose an enhanced clamp device that reduces stress concentrations in the clamp region.

(2) Analyze and asses the behavior of short glass fiber reinforced cement-based matrix subjected to tensile loading from the probabilistic point of view.

1.3 Overview of the dissertation

The probabilistic model of the yarn strength developed in this thesis is an extension of the classical Daniels' statistical fiber bundle model [16]. It includes the effects of friction between individual filaments in the bundle and represents this effect by a finite stress transfer length which causes the bundle of parallel fibers to behave like a chain of independent bundles. A method for identifying the stress transfer length based on tensile tests at various gauge lengths is presented.

Closely connected to the experimental investigation of the yarn strength is the issue of stress concentrations in the clamp region. This phenomenon causes a reduction of the measured strength compared to its theoretical value based on fiber bundle models. A new clamping device is proposed, which diminishes the stress concentration issue by a large amount.

Ultimately, the fibrous yarns are to be applied as reinforcement in composites. Cement-based fibrous composites have been thoroughly described by the author in [56, 49, 50, 54]. In this thesis, only short glass fiber reinforced concrete (GFRC) is addressed since it has not been included in the authors dissertation at the RWTH Aachen University [54]

The body of the thesis is structured as follows:

- Chapter 2: State of the art
- Chapter 3: Stress transfer length in yarns
- Chapter 4: Tensile testing of yarns
- Chapter 4: Glass fiber reinforced concrete

Summary of chapter 2

On the background of the state of the art, the length dependent strength of fibrous yarns is introduce, analyzed and issues are highlighted. Fiber bundle models, weakest link models and chain of bundles models are summarized in light of their probabilistic aspects. Current standardized tensile test setups for high-modulus multi-filament are critically discussed and both their advantages and disadvantages are pointed out motivating the development of an enhanced tensile test device.

Summary of chapter 3

A probabilistic model of the strength of fibrous yarns is derived. Based on the fiber bundle model with spatially correlated fiber strength and the chain of bundles model, it describes the length dependent yarn strength over the full range of gauge lengths with three distinguished asymptotes. These correspond to gauge ranges

1) less than the correlation length – constant mean strength;
2) greater than the correlation length and less than the stress transfer length – Weibull scaling law;
3) greater than the stress transfer length – chain-of-bundles model.

Summary of chapter 4

A new tensile test clamping device for high-modulus yarns is proposed, and the mechanism of reducing the stress concentrations is explained. Experiments with AR-glass and carbon yarns are used to validate the performance of a prototype of the new device. Standardized tensile tests using resin porters and capstan grips are performed as reference values.

Summary of chapter 5

The highly heterogeneous structure of glass fiber reinforced concrete is studied from a probabilistic point of view. A semi-analytical multiscale model of the composites response is formulated. Due to the probabilistic formulation, the model is capable

of evaluating statistical moments of the composite response and of propagating micromechanical properties of its constituents to its macro-scale behavior.

2 STATE OF THE ART

The following state of the art presents a summary and analysis of technical literature regarding fibrous yarns. Both theoretical models of their mechanical behavior and experimental setups for determining their tensile strength are described. Note that state of the art regarding glass fiber reinforced concrete is provided at the beginning of Chapter 5.

2.1 Strength of multi-filament yarns

It has been widely agreed upon in the scientific community that the strength of multifilament yarns cannot be modeled deterministically. The reasons for the use of probabilistic methods for this purpose are:

a) The random nature of fiber failure and fiber properties in general;

b) the large number of fibers (of the order of 10^4-10^8) in yarns.

If one incorporated these features in deterministic models, computational limits would be exceeded very fast [10]. In this thesis, probabilistic methods are therefore taken into account.

As shall be explained in this introductory overview to the probabilistic modeling of fibrous yarns, the yarn strength is determined by a complex propagation of the random fiber strength through the yarn structure. A yarn is a bundle of fibers with frictional interaction so that the yarn behaves essentially like a pseudo-composite. Such a structure can represented by a series-parallel system of fibers, whose strength has been addressed by many authors in the past, e.g. in [40, 19, 20, 66, 68, 50]. The elementary failure mechanism considered in this work is a micromechanical fiber rupture governed by the weakest flaw in the fiber material structure. Therefore, the weakest link model and the related Weibull scaling law, which are thoroughly described in the following subsection, can be applied.

2.1.1 Weakest link model

Weakest link models describe the strength of a structural system by the strength of its weakest link. Given that the system is divided into sub-elements where the failure of either of these elements causes the ultimate failure of the whole system, the weakest link model applies. If the sub-elements have a random strength distribution, the strength of the system decreases as its size grows. This phenomenon is known as the statistical size effect and can be explained by the behavior of global minima of sets of random realizations: with growing number of random realizations in a set the expected value of the global minimum decreases.

First intuitive formulations of the strength of materials by means of the weakest link theory and the connected statistical size effect date back to Leonardo da Vinci (1500s) and Galileo Galilei (1638). However, a robust mathematical theory with derived statistical distribution function was first formulated by W. Weibull [69].

Since a brittle filament is only as strong as its weakest cross-section, it can be assumed to behave according to the weakest link model. It is generally accepted that the random flaws in the fiber's material structure follow the compound Poisson process, i.e. the mean number of flaws per unit length with strength less than or equal σ, $\Lambda(\sigma)$ is of the form

$$\Lambda(\sigma, \sigma_0) = \left[(\sigma/\sigma_0)^m\right]/L_0 \tag{2.1}$$

where σ_0 is a scale parameter related to the reference length L_0 and m is a shape parameter [29, 45, 61, 11]. The tensile strength of fibers of length L is therefore a random variable which follows the Weibull distribution (extreme value distribution of type III) defined as

$$F(\sigma, L) = 1 - \exp\left[-L\Lambda(\sigma/\sigma_0)\right]. \tag{2.2}$$

The mean fiber strength is then

$$\mu^{\star}_{\sigma_\mathrm{f}}(L) = (L/L_0)^{-1/m}\,\sigma_0\Gamma(1+1/m) \tag{2.3}$$

with Γ denoting the gamma function. The formula reveals the length dependency of the mean fiber strength (as well as of any percentile of the fiber strength), which

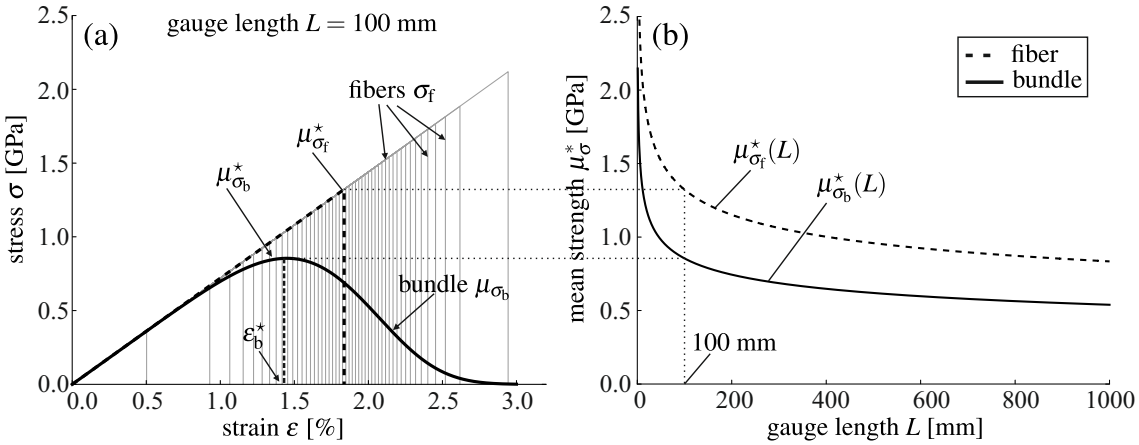

Fig. 2.1: (a) Theoretical fiber Eq. (2.8) and mean bundle Eq. (2.9) stress-strain diagrams; (b) theoretical mean fiber strength Eq. (2.3) and mean bundle strength Eq. (2.6) as a function of gauge length.

is found to be proportional to $L^{-1/m}$ (Fig. 2.1b). This means that the mean tensile strength of fibers decreases with fiber length with the slope $-1/m$ in a double logarithmic plot. For ceramic fibers used as reinforcement in composites, the shape parameter is usually between 3.0 and 7.0 [14, 12].

2.1.2 Fiber bundle models

The analysis of the strength of a fiber bundle which consists of parallel brittle fibers with random strength is based on the work of H.E. Daniels [16]. This work has been reviewed and extended with further effects relevant to fiber bundles many times since [13, 47, 10]. Daniels analyzed a set of parallel Weibull fibers (i.e. following the strength distribution given by Eq. 2.2) subjected to increasing load σ and derived an exact statistical distribution of the strength of such a bundle consisting of n_f fibers, which was later rewritten in the compact recursive form

$$G_{n_f}(\sigma) = \sum_{i=1}^{n_f} (-1)^{i+1} \binom{n_f}{i} [F(\sigma)]^i \, G_{n_f - i}\left(\frac{n_f \sigma}{n_f - i}\right) \tag{2.4}$$

where $G_0(\sigma) = 1$ and $G_1(\sigma) = F(\sigma)$ is the strength distribution of a single fiber given by Eq. (2.2). Daniels also formulated comprehensive results on the behavior of asymptotic bundles (large n_f) including the asymptotic bundle strength which

was found to be normally distributed as

$$G_{n_\mathrm{f}\to\infty}(\sigma) \approx \Phi\left(\frac{\sigma-\mu^\star_{\sigma_\mathrm{b}}}{\gamma^\star_{\sigma_\mathrm{b}}}\sqrt{n_\mathrm{f}}\right) \tag{2.5}$$

where Φ is the standard normal distribution function, $\mu^\star_{\sigma_\mathrm{b}}$ is the mean value

$$\mu^\star_{\sigma_\mathrm{b}}(L) = \sigma_0\left(\frac{mL}{L_0}\right)^{-1/m}\exp(-1/m) \tag{2.6}$$

and $\gamma^{\star 2}_{\sigma_\mathrm{b}}/n_\mathrm{f}$ the variance of the bundle strength. It is interesting to note that the mean bundle strength decreases with respect to the length with the same rate as a single fiber (i.e. $\mu^\star_{\sigma_\mathrm{b}} \propto L^{-1/m}$, see Fig. 2.1). The convergence of the mean bundle strength to its asymptotic distribution Eq. (2.5) with growing n_f was shown to be extremely slow $O(n_\mathrm{f}^{-1/6})$. Smith in [60] and later Daniels [17] himself proposed modifications on the mean value and variance that respect the actual finite number of fibers and accelerate the convergence significantly.

S. L. Phoenix and H. M. Taylor [47] analyzed the fiber bundle behavior as controlled by bundle strain ε and its failure determined by the random strain to failure of individual fibers ξ, which has the two-parameter Weibull form

$$\xi \sim F_\xi(\varepsilon, L) = \Pr\{\xi \le \varepsilon\} = 1 - \exp\left[-L/L_0(\varepsilon/\varepsilon_0)^m\right] \tag{2.7}$$

with the scale parameter ε_0 relative to the reference length L_0, and the shape parameter m. The fiber stress-strain relationship (Fig. 2.1a) is then defined as

$$\sigma_\mathrm{f}(\varepsilon) = \begin{cases} E_\mathrm{f}\,\varepsilon & : 0 < \varepsilon < \xi \\ 0 & : \text{otherwise.} \end{cases} \tag{2.8}$$

This strain based approach enables the formulation of the whole mean stress-strain curve of an asymptotic bundle ($n_\mathrm{f} \to \infty$) as

$$\mu_{\sigma_\mathrm{b}}(\varepsilon, L) = E_\mathrm{f}\varepsilon\left[1 - F_\xi(\varepsilon, L)\right] \tag{2.9}$$

on one hand and, on the other hand, additional random properties of fibers (waviness, length, modulus of elasticity etc.) can be included [47, 44, 10]. Analyzing the mean stress-strain function of a bundle (Eq. 2.9), its maximum is the mean bundle strength given by Eq. (2.6) and its stationary point is the strain at which the mean bundle strength is achieved

$$\varepsilon^\star_\mathrm{b} = \sigma_0/E_\mathrm{f}\left(\frac{mL}{L_0}\right)^{-1/m}. \tag{2.10}$$

The relation of Eq. (2.6) and Eq. (2.3) given as

$$\frac{\mu^{\star}_{\sigma_{\mathrm{b}}}}{\mu^{\star}_{\sigma_{\mathrm{f}}}} = \frac{\exp(-1/m)}{m^{1/m}\,\Gamma(1+1/m)} \tag{2.11}$$

is the reduction factor for the mean bundle strength compared to the mean fiber strength and it depends only on the Weibull modulus m. For fibers with $m \approx 5.0$ for example, the mean bundle strength is 35.5% lower than the mean fiber strength. This strength reduction is generally inherent to fiber bundles with scatter in strength of individual fibers due to micro-scale flaws.

Fiber bundle models are a means for modeling parallel structures with independent links. They can be applied to simulate the response of a fiber bundle with no interaction among individual fibers response to an applied tensile load.

2.1.3 Load sharing mechanisms

An important property of a system of parallel fibers is the stress redistribution upon local fiber damage. Existing models take this mechanical aspect into consideration by defining various load sharing patterns for surviving fibers if some fiber breaks. The nomenclature on load sharing mechanisms found in literature is not consistent. In what follows, the nomenclature used in [32] is reproduced.

The most intuitive load sharing mechanism is equal load sharing (ELS) used in the classical Daniels' fiber bundle models [16, 13], where all intact fibers take up an equal amount of the load that was carried by a failed fiber. To be more precise, the load is distributed among the intact fibers with respect to their stiffnesses. ELS assumes that fibers do not interact in parallel so that it is suitable to model dry bundles even though a weak inter-fiber friction is present [11].

In composites, the failure of a fiber might cause a stress concentration within a localized area so that the load is taken over only by close neighbors. This phenomena is called localized load sharing (LLS) which covers many models with various rules for the influence of breaks of surviving fibers in 1D, 2D and 3D [24, 25, 19, 20, 21, 22, 23, 30, 73, 63].

Load sharing rules applied e.g. by [64, 46, 15] take into consideration the longitudinal position of fiber breaks. Broken fibers then carry a residual load due to

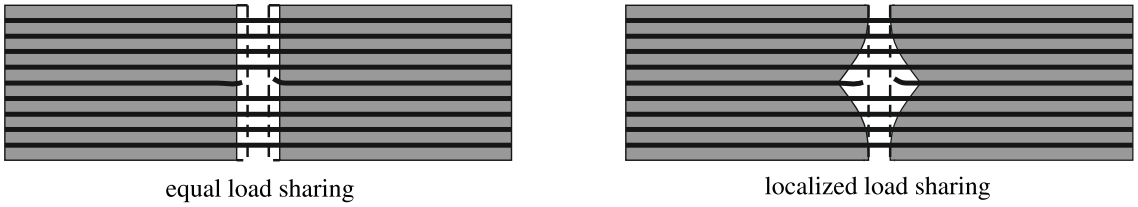

Fig. 2.2: Load sharing mechanisms

pullout and intact fibers share the remaining part of the load equally or locally. When the longitudinal position of fiber breaks and the resulting pullout is considered, the mechanism is called global load sharing (GLS) or frictional load sharing (FLS).

Localized load sharing systems are more accurate in simulating the real mechanical behavior of composites and yarns or pseudo-composites. However, LLS models are much more complex and computationally demanding than the ELS counterparts. Several factors determine whether the use of ELS can be justified for modeling of composites: 1) matrix shear stiffness 2) bond strength 3) fiber strength variability. If the matrix shear stiffness is high, the bond weak and the fiber strength variability high, ELS can be applied [46, 32]. In the other extreme case, failure will be rather localized and one of the LLS models has to be used. Pseudo-composites, which are the focus of this thesis, have extremely low frictional bond compared to polymer matrix composites. Therefore, the ELS rule is most likely to be an appropriate representation of load redistribution upon fiber failures.

2.1.4 Filament interactions in yarns

When applied as reinforcement or toughening constituent in brittle matrix composites, fibrous yarns are often not completely penetrated by the matrix. Especially in cementitious composites with fibrous reinforcement, the bond between fibers and matrix develops only in the outer region of the yarn cross-section and has a rather irregular structure. This fact alone leads to a complex damage process in a loaded crack bridge. The effect of irregularity of the outer bond on the crack bridge performance has been studied using the statistical fiber bundle model in [56, 49, 50, 10, 67].

Due to an incomplete penetration of the matrix into the yarn there is still a large fraction of filaments without any contact to the matrix.

Even though the filament-filament frictional stress is much lower than the bond shear stress transmitted by filament-matrix bond, the effect of the inner bond on the macroscopic performance of a composite cannot be neglected [26]. While the outer bond affects the behavior locally at the length scale of a crack-bridge, the inner bond influences the failure process at the length scale of a structural element with sufficiently large stress transfer (or anchorage) length. This can be documented by a significant contribution of the inner bond to the stress level in the post-cracking regime of a tensile specimen reinforced with AR-glass yarns [27]. As a consequence, the interaction and damage effects for both outer and inner bond require a detailed mechanical characterization.

While it is possible to study and characterize the interaction between a single filament and the matrix experimentally using the pull-out test [6], it is impossible to directly test the *in-situ* filament-filament interaction. An indirect qualitative experimental observation of the *in-situ* filament interaction is possible by imposing various levels of twist during the yarn tensile test. An experimental study of the effect of increased *in-situ* filament interaction on the strength of high-modulus multifilament yarns (carbon and AR-glass) can be found in [9]. A multivariate experimental analysis was used to study the compound effect of the loading rate, gauge length, fineness and twist.

A numerical approach based on Monte Carlo simulation of random filament strength was used in [51, 41] to compute the strain-stress relationship of twisted blended yarns. The stress transfer length occurring in such a yarn structure was computed as a function of yarn strain, twist level (lateral pressure), position of a filament within the bundle cross-section and filament type. An advanced model for the statistical strength of twisted fiber bundles has been presented recently in [48]. These approaches are, however, computationally very demanding.

In this thesis, the available theoretical framework of statistical fiber bundle models is utilized with the goal to provide a method for identifying the filament-filament interaction within the yarn using the data from a specifically designed tensile test

setup [9, 11, 55].

2.2 Tensile testing

In order to validate any model of tensile strength of high-modulus multifilament yarns, an appropriate tensile test device has to be used for the experiments. The steadily growing application of technical yarns has evoked intensive efforts to improve the quality and reproducibility of strength characterization for this type of material [2, 53]. In contrast to traditional yarn materials like cotton and polyester, high-modulus yarns made of glass, carbon, aramid or UHMPE are very sensitive to stress concentrations due to their brittleness when loaded in tension. At the same time, they exhibit a pronounced strength size effect due to the presence of randomly distributed flaws along the yarn. Both these properties make the use of traditional setups for yarn tensile testing difficult.

Two categories of methods that are currently being used for introducing the tensile load into a high-modulus multifilament yarn in order to measure its tensile strength are outlined below.

2.2.1 Load transfer via deflection and friction

The first category uses mechanical fixing clamps and an additional deflection of the yarn which introduces the load to the yarn through friction. The deflection reduces the force which has to be taken up by the fixing clamps. An example of this method is the test with capstan grips [2, 1, 3] where the yarn is deflected or twisted around a spool, see Fig. 2.3a.

In some cases, the tests are semi or even fully automatic (Statimat 4U with 'big bollards', Textechno GmbH) which is a great advantage of this test method. However, the method also has some disadvantages. Due to the radii of the deflection elements, the minimum test length of the specimen is limited. Furthermore, the test length of the yarn is not precisely defined since the force is introduced over a certain length at the deflection elements. Since the yarn strength is length-dependent, the test length needs to be known for the interpretation of the yarn tensile properties.

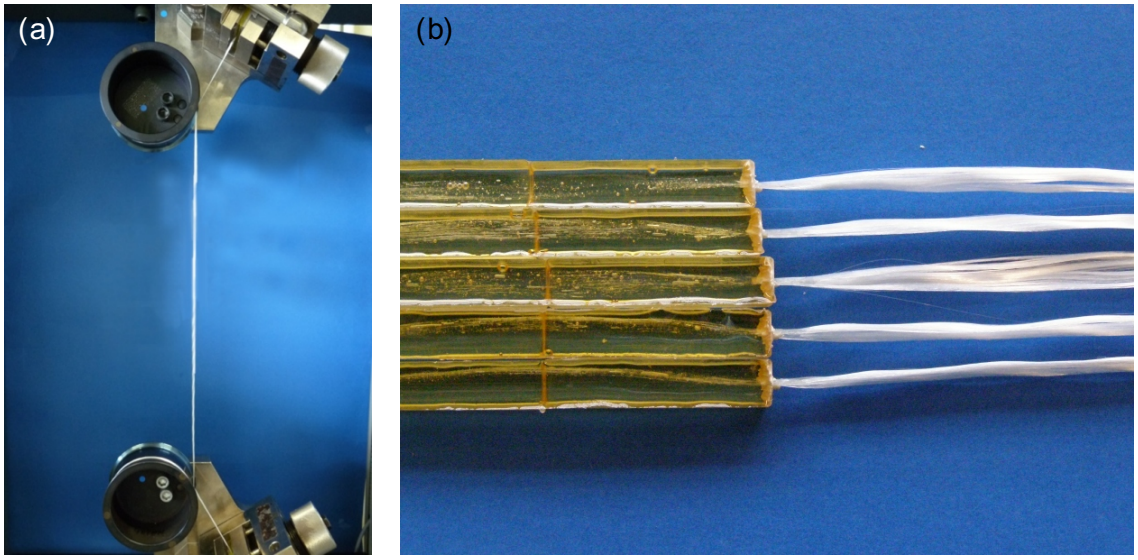

Fig. 2.3: Yarn tensile test with capstan grips – Zwick Roell AG (a); embedding the porters in resin (b) – specimens can be tested with any tensile test machine (ITA, RWTH university, Aachen, Germany

The main disadvantage, however, is the non-uniformly distributed stress among filaments. This issue arises because filaments directly contacting the spool carry more of the introduced load.

2.2.2 Load transfer via resin porters

For the second category of methods, the yarn ends are embedded in resin blocks which are then used for the load introduction (Fig. 2.3b). An example of resin porters for testing AR-glass yarns can be found in [53, 9]. The main advantage of these methods is the relatively well-defined test length and the uniform load introduction at large test lengths [67, 9]. However, the sample preparation is very

Tab. 2.1: State of the art for tensile test methods.

method	gauge length	load introduction	specimen preparation
capstan grips	not accurately defined	non-uniform	automatic
resin porters	defined gauge length	uniform	time consuming

time consuming and biased by the human factor. On one hand, manipulation during the sample preparation inevitably causes damage of the brittle filaments and, on the other hand, the inclination of the yarn to the resin porters axis is variable and induces bending into the yarn. The main advantages and disadvantages of these commonly used methods are briefly summarized in Tab. 2.1.

3 STRESS TRANSFER LENGTH IN YARNS

As stated in Sec. 2, the stress transfer length is a property of fibrous yarns, which governs their size effect behavior at longer gauge lengths, see Fig. 3.1. Therefore, it is highly important to identify this property in order to describe the tensile strength for an arbitrary length.

The key idea of the identification of the stress transfer length introduced in this thesis is to exploit the fact that the *in-situ* filament-filament interaction affects the length-dependent strength of the yarn (size effect curve). The effect of friction between filaments becomes significant when the specimen length is greater than the stress transfer length, i.e. the length at which a broken filament recovers its stress within the gauge length. Such a yarn structure becomes fragmented into a chain-of-bundles and behaves like a pseudo-composite and the slope of the size effect curve is decreased, see Fig. 3.1.

It is to be understood that the chain-of-bundles model is a simplified representation of the complex mechanics of fiber interactions. The fundamental assumption of the model is that due to the stress transfer between fibers, the yarn behaves like a chain of independent fiber bundles whose lengths equal the stress transfer length. Even though the bulk of probabilistic models of unidirectional composites are based on the chain-of-bundles assumption, the stress transfer length cannot be directly related to the length along which the fiber stress is fully recovered from a

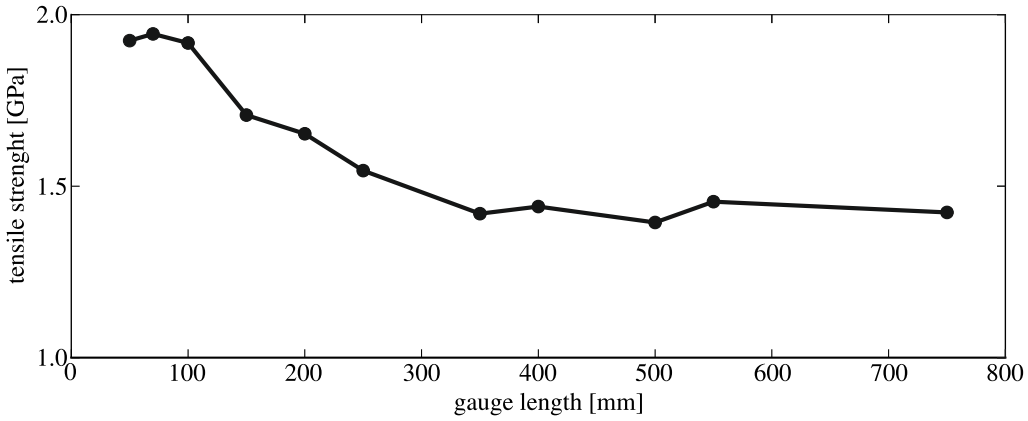

Fig. 3.1: Tensile strengths of Toho Tenax 1600 tex carbon yarns as measured at various gauge length.

rupture. Rather, the stress transfer length is a smeared representation of this physical property which is variable among filaments. For this reason, we will refer to it as 'effective bundle length'.

3.1 Model assumptions

The only source of randomness considered in the present model is the variability in local filament strength. Filaments respond elastically to tensile loading with brittle failure upon reaching their strength. The local random breaking strain ξ at a certain point over the filament length is considered to follow the Weibull distribution:

$$F_\xi(\varepsilon) = \Pr\{\xi \leq \varepsilon\} = 1 - \exp\left[-\left\langle \frac{\varepsilon}{s} \right\rangle^m\right] \tag{3.1}$$

where s and m are the scale and shape parameter of the local distribution and ε is the imposed axial strain. The spatial distribution of the random strength along a filament has a length scale l_ρ at which the strength variability diminishes [67]. As a consequence, for short specimens $l \ll l_\rho$ the strength realization along the filament can be considered a constant function with random value and, therefore, the random filament strength for this length range is length-independent. On the other hand, for $l \gg l_\rho$ the local strength varies over the filament length. Therefore, the overall filament strength is defined by the minimum local strength along the filament length corresponding to the weakest link model and is well described by the Weibull extreme value distribution [69, 67].

With these assumptions for a single filament a qualitative profile of the mean size effect curve of a fibrous yarn can be expected as shown in Fig. 3.2. Two types of mechanisms of load transfer can be distinguished depending on the yarn length. The two regions are separated by the effective bundle length (related to the stress transfer length) $l_{\mathrm{b}}^\star$ at which the fiber fragmentation can occur. The implicit assumption is that the autocorrelation length of the random strength process along the filament is less than $l_{\mathrm{b}}^\star$. This assumption is reasonable because the autocorrelation length is of the order of a few millimeters [10] while the effective bundle length in dry yarns is of the order of tens of centimeters [40, 11], see also Fig. 3.1. The two main regimes can be characterized as follows:

- For the range of lengths $l < l_{\mathrm{b}}^{\star}$, the yarn is acting as a bundle or a set of parallel, independent filaments with identical Weibull strength distribution. Its size effect behavior has been described in a large number of scientific publications, e.g. [16, 13, 44] and corrections to the asymptotic strength distribution for finite number of fibers have been proposed in [60, 17]. In such a bundle, a filament is assumed to break only once within its length and the associated released force is redistributed evenly among the surviving fibers according to the equal load sharing mechanism, see Sec. 2.1.3. Two limiting behaviors of a bundle with independent filaments can be distinguished based on the dependence of strengths of individual filaments on their length.
    - For very short lengths $l < l_{\rho}$ any realization of the random process of local strength along the filament can be considered a constant function. In other words, the realization of the local filament strength simplifies to a single random variable independent of the position along the filament. The consequence is that the left asymptote of the filament mean strength is a horizontal line at the level of the mean value of the local random filament strength. Therefore, also the mean size effect curve of a bundle has a horizontal left asymptote [66, 67]. As the bundle length approaches the correlation length l_{ρ} the mean size effect curve starts to decline from the left horizontal asymptote and turns slowly down in the direction of the middle asymptote dictated by the classical Weibull size effect [69].
    - Bundles with length greater than l_{ρ} but still shorter than $l_{\mathrm{b}}^{\star}$ are assumed to consist of non-interacting fibers whose strength is described by the weakest link model and Weibull scaling based on the classical extreme value theory. The slope $-1/m$ of the middle asymptote in log-log scale is dictated solely by the shape parameter m of the Weibull distribution of the local filament strength.
- With increasing gauge length, the filament-filament friction can recover the stress released upon a filament break and allows for multiple filament breaks resulting in fragmentation of filaments along their lengths. Such a length $l_{\mathrm{b}}^{\star}$ marks the transition from the bundle behavior to the behavior of a chain-of-

bundles. The slope of the mean size effect curve for $l > l_{\mathrm{b}}^{\star}$ is significantly reduced. Asymptotically, its slope approaches $-1/(n_{\mathrm{f}}m)$, where n_{f} is the number of filaments in the yarn [23]. The particular shape of this transition depends on the number of filaments in the bundle [19, 20].

The transition zone from a bundle range to chain-of-bundles range is of special interest. The change in the slope of the size effect curve reveals the length $l_{\mathrm{b}}^{\star}$ at which the fragmentation starts. The idea of the present paper is to exploit this fact in order to identify the effective bundle length $l_{\mathrm{b}}^{\star}$ within the tested yarn. The identification procedure tries to find an intersection between the two branches of the mean size effect curve. The mathematical formulation of the two branches is summarized in the following two sections.

3.2 Bundle of parallel independent fibers

As derived in Sec. 2, the mean strength of a single Weibullian filament is prescribed as

$$\mu_{\sigma_{\mathrm{f}}} = s_0 \cdot \left(\frac{l_0}{l}\right)^{-1/m} \cdot \Gamma\left(1 + \frac{1}{m}\right) \tag{3.2}$$

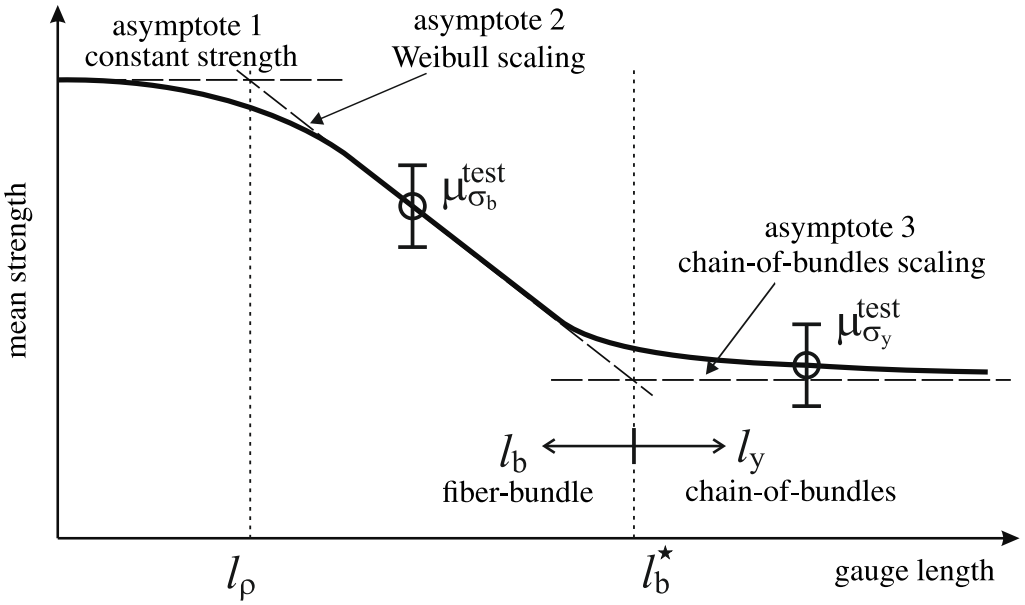

Fig. 3.2: Mean size-effect curve in log-log scale with three distinguished asymptotes

with s_0 and m denoting the scale and shape parameters of the Weibull distribution, respectively, and $\Gamma(\cdot)$ is the Gamma function [13]. The scale parameter s_0 is related to a reference length l_0. As pointed out in [67] the above power-law scaling predicts unlimited mean strength for $l \to 0$ and is therefore unrealistic. To impose an upper bound on the strength, a statistical length scale in the form of an autocorrelation length of a random strength process along the filament has been introduced in [67]. With this in mind, the length-dependent mean filament strength given by Eq. (3.2) can be formulated with the variable l_ρ. The resulting form then includes the function $f_\rho(l_\rho, l)$ as:

$$\mu_{\sigma_\mathrm{f}} = s_0 \cdot f_\rho\left(l_\rho, l\right) \cdot \Gamma\left(1 + \frac{1}{m}\right) \tag{3.3}$$

The refined scaling function $f_\rho(l_\rho, l)$ accounting for the correlation length l_ρ has been suggested as either

$$f_\rho\left(l_\rho, l\right) = \left(\frac{l}{l_\rho} + \frac{l_\rho}{l_\rho + l}\right)^{-1/m} \tag{3.4}$$

or

$$f_\rho\left(l_\rho, l\right) = \left(\frac{l_\rho}{l_\rho + l}\right)^{1/m}. \tag{3.5}$$

Note that this length-scaling remains qualitatively unchanged for any arbitrary number of parallel filaments. Thus, in the sequel the length dependency of the scaling parameter within the range $l_\rho < l_\mathrm{b} < l_\mathrm{b}^\star$ (see Fig. 3.2) shall be represented by the scaling function

$$s_\mathrm{b} = s_0 \cdot f_\rho\left(l_\rho, l_\mathrm{b}\right). \tag{3.6}$$

In the limit of $l \gg l_\rho$, the scaling in Eqs. (3.4) and (3.5) recovers the classical Weibull length-dependency $f_\mathrm{W}\left(l\right) = \left(l_\rho/l\right)^{1/m}$. Such a decomposition of the length effect allows for a simple scaling of the mean value

$$\mu_{\sigma_1} = \mu_{\sigma_0} \cdot \frac{f_\rho\left(l_1\right)}{f_\rho\left(l_0\right)} \tag{3.7}$$

that shall be used later in the identification procedure.

The cumulative distribution function of a random per fiber bundle strength of a parallel set of filaments with independent identically distributed strength, $G_{n_\mathrm{f}}(\varepsilon)$, is given by the recursive formula Eq. (2.4), derived by Daniels [16]. The resulting bundle strength approaches the Gaussian normal distribution, $G_{n_\mathrm{f}\to\infty}$ given by

Eq. (2.5), as the number of filaments grows large ($n_\mathrm{f} \to \infty$). Based on Daniels' analysis, the expected asymptotic mean bundle strength μ_{σ_b} with Weibull fibers is related to the filament properties as

$$\mu_{\sigma_\mathrm{b}} = s_\mathrm{b} \cdot m^{-1/m} \cdot c_m \quad \text{with} \quad c_m = \exp\left(-\frac{1}{m}\right) \tag{3.8}$$

with s_b obtained using Equation (3.6). The standard deviation $\gamma_{\sigma_\mathrm{b}}$ is given as

$$\gamma_{\sigma_\mathrm{b}} = s_\mathrm{b} \cdot m^{-1/m} \sqrt{c_m \cdot (1 - c_m)}. \tag{3.9}$$

The (length-dependent) standard deviation of yarn random strength is scaled in the same way as the mean value is scaled in Eq. (3.7). As a consequence, the coefficient of variation of the bundle strength does not depend on the bundle length. The decrease of the normalized mean bundle strength μ_{σ_b} with respect to the filament strength μ_{σ_f} is obvious from the comparison of Eqs. (3.8) and (3.2). In reality, bundles have a finite number of filaments n_f and the mean strength is thus only approaching the Daniels' asymptotic prediction. Both Smith and Daniels proposed ways to decrease the gap between the strength distribution of finite sized bundles and the asymptotic Daniels' normal approximation by adjusting μ_{σ_b} to $\mu_{\sigma_{\mathrm{b,n_f}}}$ [60, 17]. Both adjustments have a similar form so that only Smith's formula is written below for demonstration purposes:

$$\mu_{\sigma_{\mathrm{b,n_f}}} = \mu_{\sigma_\mathrm{b}} + n_\mathrm{f}^{-2/3} b \cdot \lambda. \tag{3.10}$$

In the case of Weibull filament distribution the parameter

$$b = s_\mathrm{b} \cdot m^{-1/m-1/3} \exp\left[-1/\left(3m\right)\right]$$

and the coefficient $\lambda = 0.996$. This correction shifts the mean value of the bundle strength. The standard deviation corresponding to μ_{σ_b} given by Eq. (3.9) is a fair approximation and does not need any further adjustment for a finite number of filaments n_f.

3.3 Chain of fiber bundles

Filaments in yarns are not ideally independent as assumed by the fiber bundle models. They exhibit a certain amount of frictional interaction that leads to multiple

rupture of individual filaments. The distance between two breaks along a filament can only be larger than the stress transfer length, also called the ineffective or shielded length. This length determines the distance from a break beyond which the filament stress state is independent of further ruptures. Based on this reasoning, the mechanical-probabilistic model represents the yarn with interacting fibers as a chain of mechanically and statistically independent fiber bundles or chain-of-bundles. Each bundle is assumed to have the length corresponding to the stress transfer length. A yarn can therefore be idealized as a one-dimensional chain of independent identically distributed bundles with equal load sharing within each bundle.

The strength distribution $G_{n_\mathrm{f}}(\varepsilon)$ of each of the serially coupled bundles subjected to the longitudinal global strain ε, has been described in Sec. 3.2. Obviously, the yarn strength is governed by the weakest bundle and thus it is distributed as follows

$$H_{n_\mathrm{b},n_\mathrm{f}}(\varepsilon) = 1 - \left[1 - G_{n_\mathrm{f}}\left(\varepsilon\right)\right]^{n_\mathrm{b}}, \quad \varepsilon \geq 0 \tag{3.11}$$

with n_b being the number of serially coupled bundles.

The distribution of the chain-of-bundles strength can have different shapes depending on the ratio between the number of filaments n_f and number of bundles n_b [62, 66]. In general, its left tail is of the Weibull form and, close to the mean value, the distribution can be approximated by the Gaussian normal form. For small values of n_f, the lower (Weibull) tail of the bundle strength distribution reaches close to its mean value. On the other hand, for large n_f, the Gaussian shape of the distribution reaches far into the lower tail.

As known from the extreme value theory, the minimum of IID Gaussian variables, here representing the strength of a chain-of-bundles with dominating Gaussian distribution, approaches the Gumbel distribution [18] as $n_\mathrm{b} \to \infty$

$$H_{n_\mathrm{b},n_\mathrm{f}}(\varepsilon) = 1 - \exp\left[-\exp\left(\frac{\varepsilon - b_{n_\mathrm{b},n_\mathrm{f}}}{a_{n_\mathrm{b},n_\mathrm{f}}}\right)\right] \tag{3.12}$$

where

$$a_{n_\mathrm{b},n_\mathrm{f}} = \frac{\gamma_{\sigma_\mathrm{b}}}{\sqrt{2\omega}},$$

$$b_{n_\mathrm{b},n_\mathrm{f}} = \mu_{\sigma_\mathrm{b},n_\mathrm{f}} + \gamma_{\sigma_\mathrm{b}}\left[\frac{\ln\left(\omega\right) + \ln\left(4\pi\right)}{\sqrt{8\omega}} - \sqrt{2\omega}\right]$$

and $\omega = \ln(n_\mathrm{b})$. The mean value of yarn strength is then $\mu_{\sigma_\mathrm{y}} = b_{n_\mathrm{b},n_\mathrm{f}} - \eta \cdot a_{n_\mathrm{b},n_\mathrm{f}}$ and the median equals $b_{n_\mathrm{b},n_\mathrm{f}} + \ln(\ln(2)) \cdot a_{n_\mathrm{b},n_\mathrm{f}}$. Here, $\eta \approx 0.5772$ denotes the Euler-Mascheroni constant. The strength distribution given in Equation (3.12) is very accurate for a high number of filaments, n_f, and a number of bundles greater than approximately 300. For lower numbers of bundles $n_\mathrm{b} \in (1; 300)$, a cubic regression, which was proposed in [66], will be assumed for the mean chain-of-bundles strength. Using the constants introduced in Eq. (3.11), the cubic regression can be written as

$$\mu_{\sigma_\mathrm{y}} = \mu_{\sigma_\mathrm{b}} - \gamma_{\sigma_\mathrm{b}} \left(-0.007\omega^3 + 0.1025\omega^2 - 0.8684\omega\right), \tag{3.13}$$

where μ_{σ_b} and $\gamma_{\sigma_\mathrm{b}}$ are the bundle mean strength and standard deviation, respectively. This approximation describes the transition from the mean value of the Gaussian distribution of a single bundle to the mean value of the Gumbel distribution of a chain-of-bundles.

As already mentioned, for the strength distribution of bundles consisting of a low number of filaments n_f the left Weibull tail reaches close to the mean value. As a consequence, the Weibull shape of the distribution becomes significant also for the distribution of the chain-of-bundles strength. Yarns consisting of a very large number of such bundles (of the order 10^3 bundles with 8 parallel filaments) have the Weibull strength distribution with the Weibull modulus given solely by multiplying the number of filaments n_f by the Weibull modulus of a single filament m [19, 20].

For the considered types of multifilament yarns consisting of several hundreds of filaments and a low number of bundles per meter (approximately 5 for AR-Glass, 2400 tex) it is sufficient to use the approximating Eq. (3.13) or the median value obtained from:

$$\sigma_y^{50} = \mu_{\sigma_{\mathrm{b},\mathrm{n_f}}} + \gamma_{\sigma_\mathrm{b}} \Phi^{-1}\left(1 - 0.5^{1/\mathrm{n_b}}\right). \tag{3.14}$$

Here, $\Phi^{-1}(\cdot)$ stands for the inverse standard Gaussian cumulative distribution function (percent point function) and $n_\mathrm{b} = l_\mathrm{y}/l_\mathrm{b}$ stands for the number of bundles the yarn consists of.

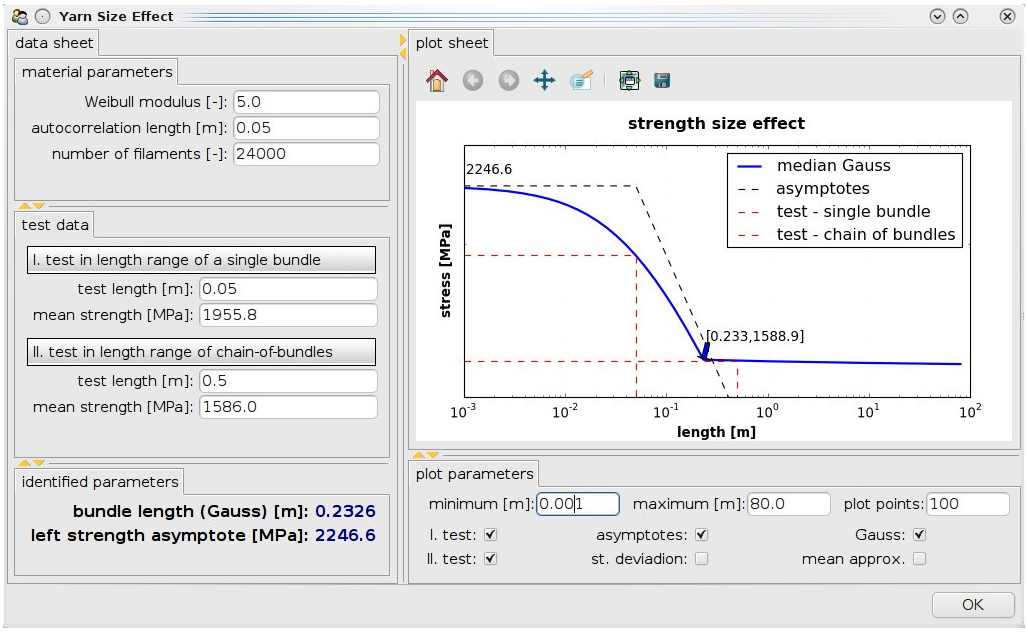

Fig. 3.3: Example of the effective bundle length identification with software module implemented in Python scripting language.

3.4 Evaluation of the effective bundle length

Let us assume that two sets of strength data $\mu_{\sigma_\mathrm{b}}^{\mathrm{test}}$ and $\mu_{\sigma_\mathrm{y}}^{\mathrm{test}}$ are available for two respective gauge lengths falling into the different length ranges defined in Sec. 3.1, i.e. $l_\mathrm{b}^{\mathrm{test}} < l_\mathrm{b}^\star$ and $l_\mathrm{y}^{\mathrm{test}} > l_\mathrm{b}^\star$. Apart from the known gauge lengths and the measured mean strengths, the knowledge of the Weibull modulus m and correlation length l_ρ are required. The estimation of the effective bundle length $l_\mathrm{b}^\star$ is then performed using the following procedure (see Fig. 3.3 for the user interface of the implemented identification module).

1. The mean strength $\mu_{\sigma_\mathrm{b}}^{\mathrm{test}}$ estimated as the average strength for the length $l_\mathrm{b}^{\mathrm{test}}$ is substituted into Eqs. (3.8) and (3.10) in order to obtain the scaling parameter s_b of the Weibull distribution for the tested length

$$s_\mathrm{b} = \mu_{\sigma_\mathrm{b}}^{\mathrm{test}} \cdot \left[m^{-1/m} \cdot \mathrm{c} + n_\mathrm{f}^{-2/3} \cdot \; m^{-(1/m+1/3)} \exp\left(-\frac{1}{3m}\right) \lambda \right]^{-1}. \tag{3.15}$$

2. With the scaling parameter s_b at hand, the corresponding standard deviation $\gamma_{\sigma_\mathrm{b}}$ is evaluated using Equation (3.9). It is important to emphasize, that we use the theoretical scatter of the bundle strength to identify the slope of the mean size effect curve in the range of lengths $l \in \langle l_\rho; l_\mathrm{b}^\star \rangle$ instead of the measured

value of scatter. Note that in a typical yarn the number of filaments n_f is very large and thus the theoretical scatter of the bundle strength is very small (proportional to $n_\mathrm{f}^{-1/2}$).

The choice of the theoretical scatter of the bundle strength is justified by the fact that the experimentally obtained standard deviation is increased by the sources of randomness other than the scatter of local strength along the filaments. Obviously, this was also the case in the performed tests, as the measured variability did not correspond to the slopes of the means ize effect curve for the two tested types of yarns. This discrepancy was ascribed to the manual production of the specimens and clamps [9, 50]. Note that even if a realistic measurement of the scatter of the yarn strength due to the random filament strength was possible, much larger sample size would be required for a statistically significant estimate of the second moment compared to the estimate of the mean yarn strength.

3. The obtained bundle characteristics are scaled to the unknown length $l_\mathrm{b}^\star$ using Equation (3.7) and exploiting the fact that the standard deviation (as well as every quantile) scales identically with the mean value:

$$\mu_{\sigma_\mathrm{b}}^\star = \mu_{\sigma_\mathrm{b}}^\mathrm{test} \cdot \frac{f\left(l_\mathrm{b}^\star\right)}{f\left(l_\mathrm{b}^\mathrm{test}\right)} \text{ and } \gamma_{\sigma_\mathrm{b}}^\star = \gamma_{\sigma_\mathrm{b}}^\mathrm{test} \cdot \frac{f\left(l_\mathrm{b}^\star\right)}{f\left(l_\mathrm{b}^\mathrm{test}\right)}.$$

4. The chaining effect involved in the experimental data is now expressed using Equation (3.13) for the unknown bundle length $l_\mathrm{b}^\star$ as

$$\mu_{\sigma_\mathrm{y}}^\mathrm{test} = \mu_{\sigma_\mathrm{b}}^\star(l_\mathrm{b}^\star) - \gamma_{\sigma_\mathrm{b}}^\star\left(-0.007\omega_\star^3(l_\mathrm{b}^\star) + 0.1025\omega_\star^2(l_\mathrm{b}^\star) - 0.8684\omega_\star(l_\mathrm{b}^\star)\right) \quad (3.16)$$

where $\omega_\star$ represents the logarithm of the number of bundles in series $\omega_\star = \ln\left(l_\mathrm{y}^\mathrm{test}/l_\mathrm{b}^\star\right)$. The non-linear implicit Eq. (3.16) is then solved for $l_\mathrm{b}^\star$ using standard root finding algorithms.

In order to demonstrate the identification procedure on real data, two test series with different yarn types (carbon and AR-glass) have been conducted. The input data and the results of the evaluation are summarized in Tab. 3.1. The resulting effective bundle length for AR-glass yarns is one third larger than that of the carbon yarn detecting a higher amount of frictional interaction within the carbon yarn. This

property	unit	symbol	carbon	AR-glass
fineness	[tex]	-	1600	2400
No. of filaments	[-]	n_f	24000	1600
Weibull modulus	[-]	m	5.00	4.52
correlation length	[mm]	l_ρ	1.0	1.0
gauge length I	[mm]	$l_\mathrm{b}^\mathrm{test}$	50.0	100.0
measured strength I	[MPa]	$\mu_{\sigma_\mathrm{b}}^\mathrm{test}$	1955.8	1038.0
gauge length II	[mm]	$l_\mathrm{y}^\mathrm{test}$	500.0	500.0
measured strength II	[MPa]	$\mu_{\sigma_\mathrm{y}}^\mathrm{test}$	1586.9	882.8
identified bundle length	[mm]	$l_\mathrm{b}^\star$	142.1	201.8

Tab. 3.1: Summary of experimental data and the evaluated effective bundle lengths for carbon and AR-glass yarns.

trend is in agreement with experimental observation. On one hand, in the post-peak behavior of a tensile test, the level of stress transmitted by friction is significantly higher for carbon yarns than for AR-glass yarns. On the other hand, the mean size effect curve tends to flatten at smaller gauge lengths for carbon than for AR-glass yarns.

3.5 Remarks to the identification method

Due to the limitations of the experimental setup, the described procedure can be considered valid only in a certain range of gauge lengths. The following limiting cases must be considered when designing the test series with the goal of identifying the effective stress transfer length.

- The identification procedure is valid only if the effective bundle length to be identified (the intersection point of the single bundle and a the chain-of-bundles size effect curves) is between the two test lengths $l_\mathrm{b}^\mathrm{test}$ and $l_\mathrm{y}^\mathrm{test}$, i.e. if the sought length $l_\mathrm{b}^\star \in \left\langle l_\mathrm{b}^\mathrm{test}; l_\mathrm{y}^\mathrm{test} \right\rangle$.
- If the correlation length is of the same order as the test length ($l_\mathrm{b}^\mathrm{test} \approx l_\rho$) the

estimation of $l_{\mathrm{b}}^{\star}$ becomes sensitive to slight changes in l_{ρ}. In particular, for the identification summarized in Tab. 3.1, the correlation length $l_{\rho} = 1.0\,\mathrm{mm} \ll l_{\mathrm{b}}^{\mathrm{test}} = 50\,\mathrm{mm}$ was assumed leading to $l_{\mathrm{b}}^{\star} = 142.1\,\mathrm{mm}$ for the carbon yarns. When assuming the autocorrelation length in the same length range as the short test length, e.g. $l_{\rho} = l_{\mathrm{b}}^{\mathrm{test}} = 50\,\mathrm{mm}$, the estimated bundle length is $l_{\mathrm{b}}^{\star} = 226.0\,\mathrm{mm}$. A possible remedy would be to add further test(s) in the range between the $l_{\mathrm{b}}^{\mathrm{test}}$ and $l_{\mathrm{y}}^{\mathrm{test}}$ and to make the correlation length a part of the regression procedure.

- The identification procedure does not account for the case that the measured strength for $l_{\mathrm{b}}^{\mathrm{test}}$ is distorted by the nonuniform loading of filaments due to the irregularities in the yarn clamping. These effects lead to the reduction of the strength for short specimens as described in [67, 55]. This case can be handled by simply ignoring the short gauge length tests with a decay in mean strength. For the tested AR-glass yarns, the strength reduction could be observed experimentally for test lengths $l_{\mathrm{b}}^{\mathrm{test}} < 40\,\mathrm{mm}$.

Another point to mention is that the bundle length has been identified as a deterministic value. It might be argued that it exhibits some scatter along the yarn, i.e. that the bundles in a yarn have variable lengths [42]. The justification for the assumption of the constant bundle length can be constructed by realizing that the actual bundle length is related to the stress transfer length which in turn depends on the spatially variable filament-filament friction. In particular, two directions of spatial scatter of friction can be distinguished: along and across the yarn.

- Along the yarn: As the level of filament friction is relatively low, the stress transfer length needed to recover the breaking stress is large, at the order of centimeters. On the other hand, the length-scale of spatial variation of the filament-filament friction due to irregular packing of the yarn is at the order of micrometers. Realizing that the stress transfer length represents the sum of many local frictional links along the filament we can expect that the local scatter of friction gets homogenized at the scale of the stress transfer length. Therefore, the scatter of stress transfer length can be regarded as very small. More precisely, the fluctuating friction intensity along a single filament

can be idealized as n_c number of frictional cells with constant level of friction, each represented by independent, identically distributed (IID) random variable given by the mean μ_c and variance $\sigma_c^2 > 0$. The coefficient of variation of the cell friction is $\mathrm{cov}_c = \sigma_c/\mu_c$. As stated above, the number of frictional cells n_c along a filament within the mean stress transfer length having a significant difference in friction level is very high. Therefore, the mean value μ_f of the sum of these frictional contributions along the yarn defining the stress transfer length converges to $n_c \cdot \mu_c$ and, according to the central limit theorem (CLT), the variance is equal to $\sigma_f^2 = n_c \cdot \sigma_c^2$. As a consequence, the coefficient of variation $\mathrm{cov}_f = \sigma_c/(\sqrt{n_c} \cdot \mu_c) = \mathrm{cov}_c/\sqrt{n_c}$ rapidly decreases at a length-scale of the stress transfer length with large n_c

- Across the yarn: The scatter of friction due to variable filament surface roughness or lateral pressure within the yarn cross section diminishes as the number of filaments n_f grows large. Formally, the bundle length can be idealized as the average of filament stress transfer lengths within the cross section. All stress transfer lengths of individual filaments can be viewed as IID random variables characterized by mean μ_f and variance $\sigma_f^2 > 0$. The CLT then states that as the sample size n_f increases, the distribution of the sample average approaches the Gaussian normal distribution with mean $\mu_l = \mu_f$ and variance $\sigma_l^2 = \sigma_f^2/n_f$ irrespective of the shape of the distribution of the random variable. The coefficient of variation of the stress transfer length $\mathrm{cov}_l = \mathrm{cov}_c/\sqrt{n_c n_f}$. Thus, in the case of applied yarns the scatter of the filament transfer length can be assumed very small.

Based on these considerations the variance of the effective bundle length should become insignificant and, therefore, the assumption of a constant $l_b^\star$ along the yarn seems to be justified in the context of the experimental identification. It should be noted that the redistribution pattern included in the applied chain-of-bundles model is based on the global load sharing rule (see Sec. 2.1.3). As the chaining of bundles for lengths $l > l_b^\star$ is caused by the frictional stress along the filaments, it should also result in a more local redistribution of stresses upon a filament break. This issue is not included in the applied chain-of-bundles approximation of the corresponding

part of the mean size effect curve.

3.6 Conclusions

The known aspect of length dependency of the tensile strength of fibrous yarns has been investigated and a model has been developed with two distinguished modes of mechanical behavior. These two modes represent the asymptotic behavior for short and long yarns. For short yarns, the statistical fiber-bundle model due to Daniels applies with reasonable accuracy. A modification to this model for very short lengths has been proposed by Vořechovský for the Daniels' model predicts infinite strengths as the gauge length approaches zero.

The right asymptote of the mean size effect curve (length dependency of tensile strength) describes the chain-of-bundles behavior characteristic to fibrous composites and twisted yarns. However, even dry yarns with no twist behave like a chain-of-bundles if the gauge length is sufficiently long. Filaments can rupture multiple times and the mean tensile strength decreases with a much lower slope than during the fiber-bundle mode. This behavior is closely related to the *in situ* filament friction, which is a material property and marks the transition between the fiber-bundle and the chain-of-bundles behavior.

Upon this idea, a method based on the size effect curve has been proposed to identify the transition length marking the 'effective bundle length'. With the use of a set of standard yarn tensile tests at different gauge lengths and an analytical model of the mean size effect curve, the inter-filament frictional interaction can be indirectly identified with a moderate effort. The identification method was applied to AR-glass and carbon yarns and with the help of the implemented software module, the effective bundle lengths have been identified for these materials.

4 TENSILE TESTING OF YARNS

As stated in the state of the art Sec. 2.2, the growing market of technical textiles requires robust methods for quality management. One of the key properties of high-modulus yarns for structural applications is their tensile strength. However, the brittle fibers are prematurely damaged in the clamping systems of existing tensile test machines, see Sec. 2.2. Therefore, the measured tensile strength is underestimated making the design with the tested material overly safe and not economic. This leads to larger structural dimensions and thus wasting of both the textile and the matrix material.

To avoid stress concentrations in yarns at the clamps during the tensile test, a new clamp adapter has been developed, which separates the functions of yarn fixation and of stress homogenization (Fig. 4.1b). This novel clamp adapter for the Statimat 4U yarn tensile test machine produced by Textechno GmbH was developed in order to meet the special requirements on precise tensile testing of high-modulus multifilament yarns. With the new clamp adapter, higher strengths close to the theoretical values (perfectly clamped filaments at a unique length and with no initial

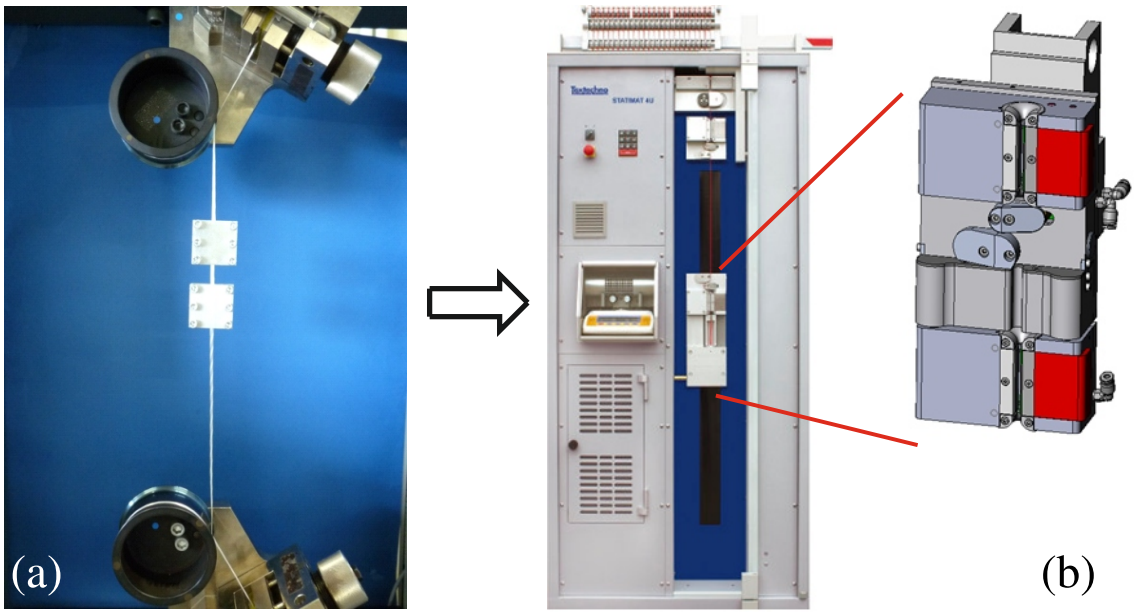

Fig. 4.1: Development of the clamp adapter: (a) first simple realization of the mechanism; (b) Prototype of the adapter produced by Textechno GmbH.

damage) can be measured. A test series comparing yarns strengths tested with the novel clamp adapter and with standard test methods has been performed and the results are discussed in this thesis. Furthermore, they are compared with theoretical values using the Daniels' fiber-bundle model.

4.1 New tensile test device

The newly developed tensile test device – a clamp adapter for the tensile test machine Statimat 4U (referred to as 'Statimat 4U adapter' further in the text) – significantly reduces the problem of stress concentration in the clamps. On the other hand, compared to the current tensile test methods, it enables the testing of yarns with precisely defined lengths so that the device can be used to measure the effect of yarn length on its strength, see Chapter 3. Up to this point, the resin porters were the only option for direct testing of the tensile strength of dry high-modulus yarns made of glass fibers. Otherwise, indirect strength measurements have been used in the industry. A common method is to test the fibers directly in the polymer matrix, i.e. to test the glass fiber reinforced composite. Such a tensile test is reasonable from the practical point of view but it tells little about the strength of the raw yarn and, therefore, can neither be used for extrapolation to other composite materials nor does it characterize the material for purposes of e.g. quality management.

The basic concept of the test set up is the separation of the clamping function from the stress homogenization function at the ends of the test length into two pairs of separate clamps controlled by separate pressure air circuits. Thanks to the introduction of the homogenizing clamp into the semi-automated Statimat 4U machine, several test series with a large number of samples for varied test lengths and yarn materials can be performed.

Tensile tests performed with the Statimat 4U adapter proceed in the following steps:

1.) The outer 'fixation clamps' (FCs) clamp the yarn with the pressure p_{FC} and introduce a fraction of the axial prestress force F_0 (see Fig. 4.2a).

2.) The yarn is laterally compressed by the inner 'homogenization clamps' (HCs)

with soft polyurethane contact layers with the pressure p_{HC} which increases the inter-filament interaction within the yarn cross-section.

3.) An additional axial force F_{HC} is introduced by the homogenization clamp. In general F_{HC} is much smaller (e.g. 1/10) than the corresponding F_{FC} (see Fig. 4.2b).

3.) The axial load F_{FC} is increased while keeping the difference between F_{FC} and F_{HC} constant, i.e. the additional axial force F_{HC} is constant (see Fig. 4.2c).

This way the yarn is not damaged by the HCs defining the gauge length since the majority of the tensile force is introduced by the outer FCs. The HCs combine lateral pressure via a soft contact layer with a moderate axial force. The lateral pressure p_{HC} homogenizes the stress in filaments by intensifying the inter-filament friction, see the stress profiles at both sides of the homogenization clamp in Fig. 4.3b. At the same time, the additional axial force F_{HC} increases the probability of filament breaks within the gauge length and thus defines the gauge length. Note that the gauge length is, contrary to the deflection-friction tests, defined as the distance between the HCs. The deflection of the yarn around the bollards of the standard Statimat 4U machine (placed between the HCs and FCs in the adapter clamp version) has a similar function as the HCs — it takes up a part of the load due to friction and can be used in addition to the HC to diminish damage in the FCs.

In contrast to the standard clamping with bollards, the control parameters (e.g. the additional axial force F_{HC} introduced by the HCs, lateral pressure p_{FC} and p_{HC} of the respective FCs and HCs) of the adapter clamps can be freely adjusted to achieve optimal test setup for a given material. If, for example, a yarn consists of brittle filaments with rather large cross-sections, they will be more prone to rupture due to the lateral pressure of the homogenizing clamp which, in this case, should be kept low in order to best balance the trade-off between homogenization of stresses within the yarn cross-section and the initial filament damage.

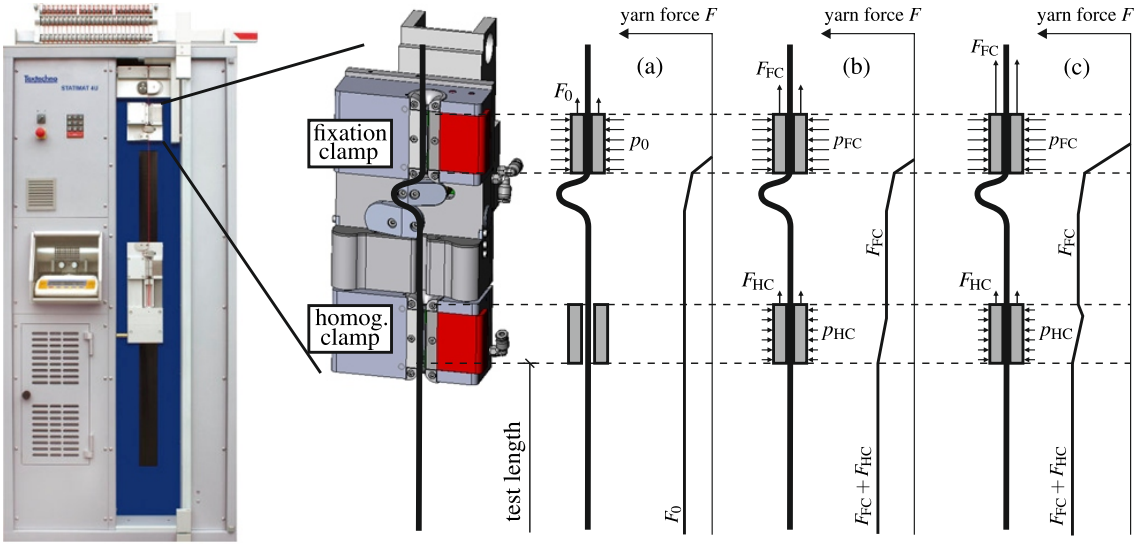

Fig. 4.2: Statimat 4U adapter with the newly developed clamp (detail): (a)-(c) phases of the tensile test with stress plotted along the tested yarn.

4.2 Comparative experiments

In order to assess the quality of the Statimat 4U adapter, tensile tests have been performed using both the adapter and standard methods for reference. Yarns of three different materials were tested.

4.2.1 Material

1.) AR-glass

Material: AR-glass yarns 1200 tex (Saint-Gobain Vetrotex Deutschland GmbH)
Reference method 1: embedding the porters in resin
Reference method 2: capstan grips
Gauge lengths adapter: 50, 70, 110, 160, 230, 340 and 500 mm
Gauge lengths reference 1: 50, 70, 110, 160, 230, 340 and 500 mm
Gauge lengths reference 2: 400, 550 and 800 mm

2.) E-glass

Material: E-glass yarns 1200 tex (PPG Industries, Inc.)
Reference method: embedding the porters in resin

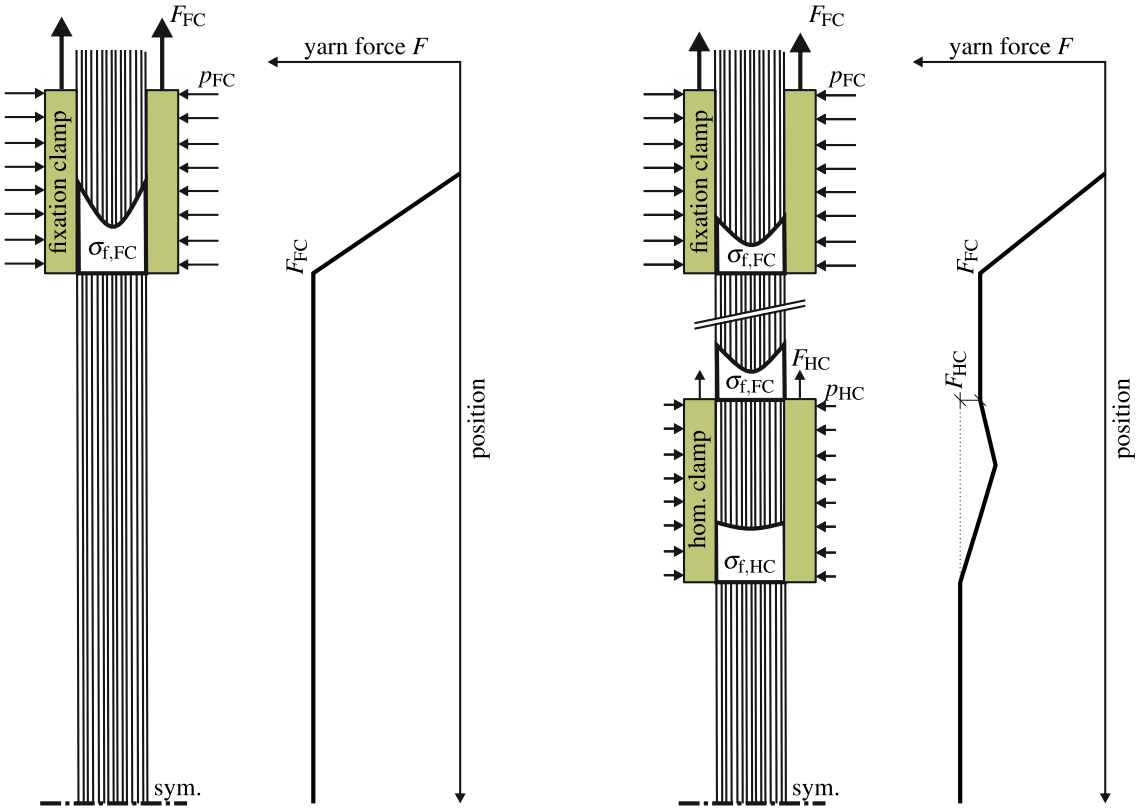

Fig. 4.3: Comparison of Statimat 4U and Statimat 4U adapter: (a) yarn stress state in the standard clamp of Statimat 4U; yarn stress state in double clamp of the Statimat 4U adapter.

Gauge lengths adapter: 50, 70, 110, 160, 230, 340 and 500 mm

Gauge lengths reference: 50, 110, 160, 230, and 500 mm

3.) carbon

Material: carbon 400 tex (Toho Tenax Co., Ltd.)

Reference method: Statimat 4U big bollard clamps

Gauge lengths adapter: 35, 70, 130, 250 and 500 mm

Gauge lengths reference: 35, 70, 130, 250 and 500 mm

4.2.2 Design of experiment

The gauge lengths were chosen, if possible, in a way that they appear equidistant in logarithmic scale. For the AR-glass tests, a randomized experiment was performed.

Initial material biases caused by fluctuations in strength due to the position of the test sample within the spool were eliminated by a random specimen choice. That means, specimens taken from the spool in an ordered manner were assigned the parameters length and test method randomly. Using the design of experiments wording [37], a block randomized comparison experiment with one factor of two levels (test method) was performed. The measured response variable was the tensile strength and the overall sample size was 280 specimens (2 levels of the factor test method, 7 blocks - gauge lengths, 20 replicates per block). The remaining two comparative experiments (E-glass and carbon) were not randomized.

Optimum parameters for testing with the Statimat 4U adapter – lateral pressure of both the HCs and the FCs and the additional axial force – were found by applying an iterative full factorial experiment design with 10 replicates for each parameter combination.

4.2.3 Discussion of the comparative experiment

The results of the comparative experiment in terms of mean strength and COV (coefficient of variation) are summarized in Fig. 4.4 and Tab. 4.1. The table summarizes the measured values and statistical significance of the hypothesis testing ($H_0 : \sigma_{uA} > \sigma_{uR}$) as well as the 95% confidence intervals (CI) for the difference of the compared methods, where σ_{uA} and σ_{uR} stand for the tensile strength measured with the Statimat 4U adapter and the reference method, respectively.

Fig. 4.4 shows that the mean tensile strengths measured with Statimat 4U adapter were for all three materials and all gauge lengths higher than the reference values. A lower level of significance for the $H_0 : \sigma_{uA} > \sigma_{uR}$ hypothesis was calculated only for the 500 mm carbon yarn tests. Carbon yarns were observed to have a much smaller scatter in strengths than glass yarns. Therefore a high level of significance of $H_0 : \sigma_{uA} > \sigma_{uR}$ is given for carbon even though the mean strength differences were not as pronounced as for AR-glass and E-glass. At the gauge length 500 mm, however, the significance of $H_0 : \sigma_{uA} > \sigma_{uR}$ was only 65% for carbon yarns. This actually suggests that an unambiguous statement on which strengths are higher cannot be given at this gauge length (the usual level of significance for

	adapter		reference			
	σ_{uA}	COV	σ_{uR}	COV	significance	95 % conf. interval
	[MPa]	[%]	[MPa]	[%]	$H_0 : \sigma_{uA} > \sigma_{uR}$	$\sigma_{uA} - \sigma_{uR}$ [MPa][%]
AR-glass 1200 tex						
50	1220	4.9	1090	10.0	≈ 1.0	(72.8, 187.0)(6.0, 15.3)
70	1224	7.3	1012	12.9	≈ 1.0	(138.9, 283.5)(11.4, 23.1)
110	1237	4.1	946	12.0	≈ 1.0	(233.6, 347.9)(18.9, 28.1)
160	1216	7.0	877	18.0	≈ 1.0	(257.3, 421.3)(21.1, 34.6)
230	1168	9.1	866	23.3	≈ 1.0	(196.8, 405.6)(16.9, 34.7)
340	1151	9.1	871	11.5	≈ 1.0	(214.2, 345.2)(18.6, 30.0)
500	1087	6.4	809	19.2	≈ 1.0	(199.3, 356.2)(18.3, 32.8)
E-glass 1200 tex						
50	1520	6.1	12405	9.7	≈ 1.0	(203.8, 357.5)(13.4, 23.5)
70	1533	5.3	1141	11.3	≈ 1.0	(247.7, 423.3)(16.8, 28.7)
110	1476	8.2	1160	12.9	≈ 1.0	(133.7, 355.1)(9.5, 25.3)
160	1405	12.2	-	-	-	-
230	1382	14.2	1066	16.2	≈ 1.0	(188.6, 443.7)(13.6, 32.1)
340	1290	13.5	-	-	-	-
500	1150	15.9	1010	20.9	0.976	(1.2, 280.3)(1.0, 24.4)
carbon 400 tex						
35	2165	3.7	1952	3.7	≈ 1.0	(159.1, 265.2)(7.3, 12.3)
70	2093	3.2	1933	3.0	≈ 1.0	(116.9, 203.1)(5.6, 9.7)
130	1936	3.6	1787	2.4	≈ 1.0	(110.2, 188.2)(5.7, 9.7)
250	1837	5.2	1694	4.2	≈ 1.0	(86.0, 201.6)(4.7, 11.0)
500	1578	6.3	1566	6.1	0.654	(-55.7, 80.8)(-3.5, 5.1)

Tab. 4.1: Results of the comparative experiments for AR-glass 1200 tex, E-glass 1200 tex, carbon 400 tex.

decision making is taken as 5%).

It seems that the differences in mean strengths for E-glass and carbon become smaller for longer gauge lengths in general. This effect is probably due to the increased influence of the statistical size effect which predicts lower strengths for yarns at longer gauge lengths because of the higher probability of severe flaws [67, 69, 16, 56]. Since the effect of stress concentrations in the clamps is constant and independent on gauge length, the failure of yarns at very long lengths is rather given by the weakest flaw in the material structure which, at some point, will exceed the strength given by the stress concentrations in the clamps. Thus the positive effect of the adapter clamps diminishes with growing length.

4.3 Comparison with theoretical strength

The fact that the new testing device could measure generally higher values of strength compared to the current techniques raised the question, whether or not the measured strength is close to the level theoretically achievable for the measured material. Using the theoretical framework of fiber-bundle models and the related statistical size effect, an analysis of the correspondence between the filament and yarn strength is performed for carbon and AR-glass.

4.3.1 Theoretical yarn strength

Let us recall the theoretical mean filament strength (Eq. 2.3) as a function of gauge length,L, given the shape m and scale (63.2% percentile) σ_0 parameters of its Weibull strength distribution (note that the scale parameter is related to the reference length L_0)

$$\mu^{\star}_{\sigma_\mathrm{f}}(L) = (L/L_0)^{-1/m}\,\sigma_0\Gamma(1+1/m). \tag{4.1}$$

This relation holds if the only source of randomness is the filament strength. See Sec. 2.1 for detailed derivation. Further, let us recall the mean strength of a fiber bundle consisting of a large number of identically and independently distributed

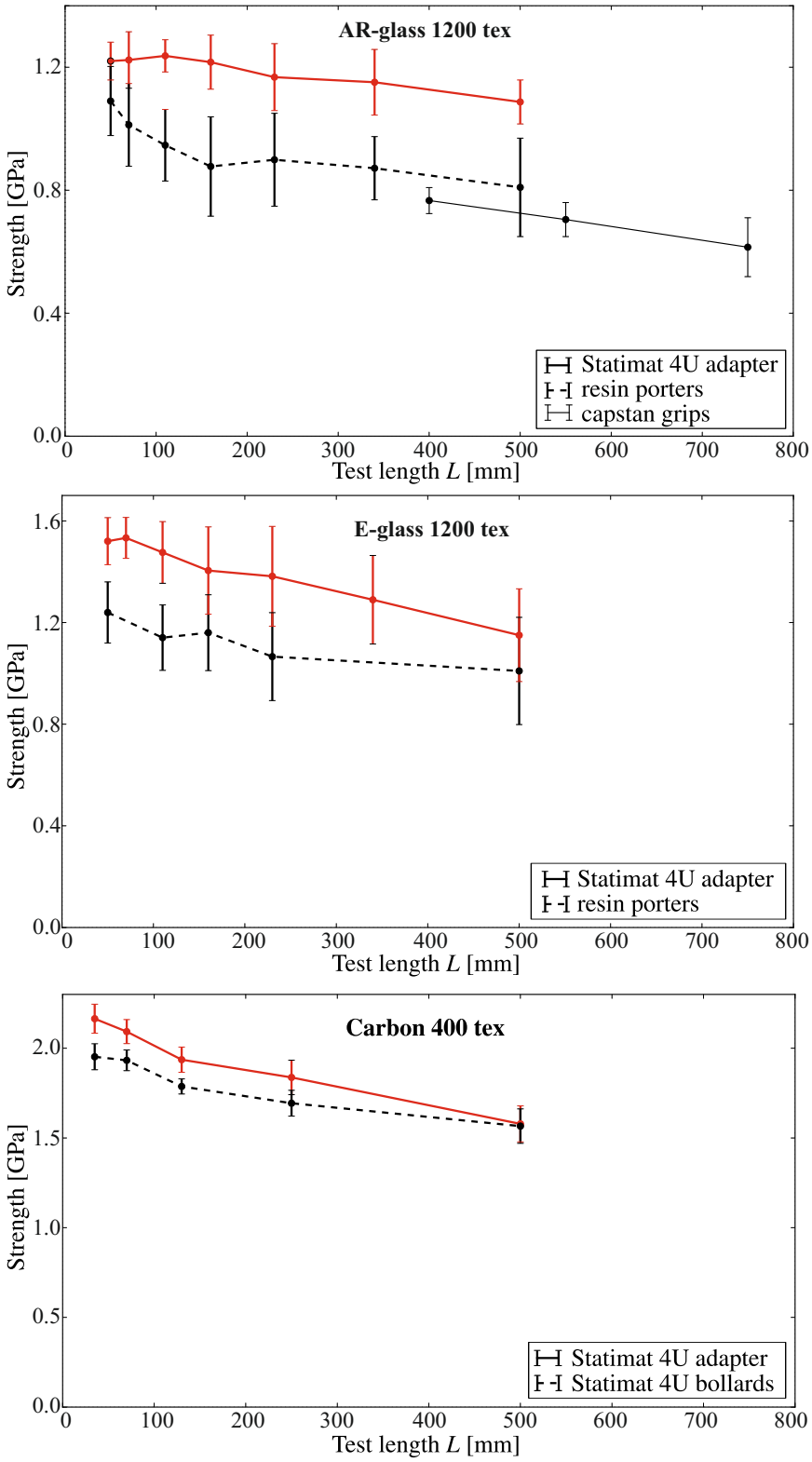

Fig. 4.4: Results of the comparative experiment: yarn strength measured with Statimat 4U adapter and various reference methods

filaments as given by Eq. 2.6

$$\mu^{\star}_{\sigma_{\mathrm{b}}}(L) = \sigma_0 \left(\frac{mL}{L_0}\right)^{-1/m} \exp(-1/m). \tag{4.2}$$

As stated in Chapter 3, this mean size effect curve only applies for a given range of gauge lengths. In this form, it includes neither the horizontal asymptote due to local strength correlation, nor the right asymptote describing the chain-of-bundles model applying for longer yarns experiencing filament fragmentation. Since both the correlation length and the effective bundle length are *a priori* unknown, we use Eq. (4.2) for the prediction of the yarn strength while keeping in mind the above statements on its accuracy for very short and very long gauge lengths.

4.3.2 Inference on the fiber strength distribution

Inference on the two unknown parameters of the filament strength distribution (shape m and scale σ_0) is drawn based on single filament tests. Tests with AR-glass and carbon filaments each at two gauge lengths were available so that the analysis is performed with these two materials only. The filament strength distribution is recalled from Sec. 2.1, Eq. 2.2 with explicit notation of the two parameters

$$F(\sigma, L) = 1 - \exp\left[-\frac{L}{L_0}\left\langle\frac{\sigma}{\sigma_0}\right\rangle\right]. \tag{4.3}$$

I. Statistical model A number of statistical models can be formulated for the available experimental data. One possibility is the filament strength distribution of the Weibull form at a fixed gauge length as given by Eq. (4.3). Parameters can be inferred for each gauge length separately and their (weighted) average then taken as the representative vector of parameters.

Another statistical model involves both sets of experiments directly via their sample means at different gauge lengths. It is prescribed by Eq. (4.1) and the model parameters are evaluated by regression.

II. Inference If the statistical model is given by Eq. (4.3), various inference methods can be used for parameter identification. Many researchers have addressed this

issue using the a) method of statistical moments; b) maximum likelihood method and c) Bayesian method [39, 28, 72, 71, 68, 61, 43, 4].

When Eq. (4.1) defines the statistical model of the data, the sought parameters have a neat interpretation in the log-log plot of the mean filament strength vs. its gauge length. The model is linear with slope $-1/m$ and its vertical position $\ln(\hat{\mu}_\sigma)$ at a log-length $\ln(\hat{L})$ is related to the logarithm of the scale parameter $\ln(\sigma_0)$ by

$$\ln(\sigma_0) = \ln(\hat{\mu}_\sigma) + \left[\ln(\hat{L}) + \ln(m/L_0) - 1\right] m^{-1} \tag{4.4}$$

resulting from Eq. (2.6).

When the parameters of the distribution of the filament strength are estimated, Eq. (4.2) can be utilized to evaluate the theoretical bundle strength at any gauge length. This computation can also be performed inversely so that the filament strength distribution at any gauge length can be evaluated when the mean bundle strengths at different gauge lengths are given.

Let us remark, that the reduction of strength for bundles compared to single filaments is in this model caused only by the scatter in filament strength. The difference between model prediction for bundle strength and measured values (in the range of gauge lengths corresponding to the bundle behavior [11]) can be related to imperfections of the test method.

4.3.3 Results

A prediction of the theoretical bundle strength (Fig. 4.5, dashed lines) based on the mean filament strength (Fig. 4.5 triangles, measured with FAVIMAT Textechno GmbH) was evaluated and compared with bundle measurements described in Sec. 4.2 (Fig. 4.5, filled circles) for AR-glass and carbon. Filament tests for E-glass were not available to the author at the time this thesis was written.

If the filament tests can be assumed to be unbiased, the predicted bundle strength (Fig. 4.5, dashed lines) fits the measured values of the yarn strength (Fig. 4.5, filled circles) fairly well in the fiber-bundle range of the yarn behavior. Even though the theoretical strength is very close to the measured strength for larger gauge lengths,

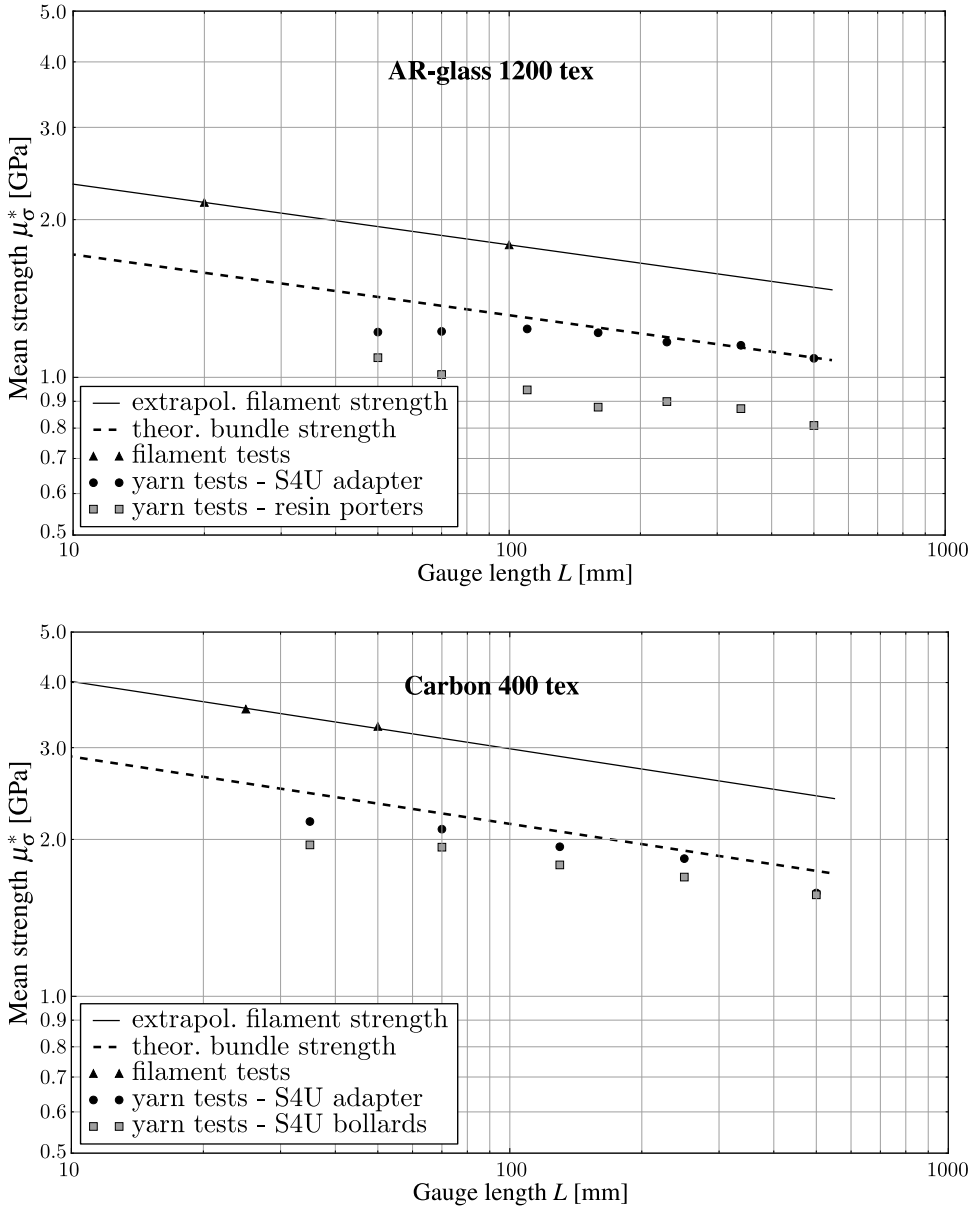

Fig. 4.5: Scaling of filament strength (solid line) and bundle strength (dashed line) based on filament tests (triangles) compared with measured bundle strengths (Statimat 4U adapter and reference method).

it has to be recalled that this rage of lengths most probably belongs to the chain-of-bundles rage of behavior while the theoretical strength is predicted for a fiber bundle with non-interacting fibers.

Compared to the the reference method (Fig. 4.5, gray squares) it is obvious that the Statimat 4U adapter delivers strengths much closer to the theoretical bundle strength, which assumes a perfect clamping and thus the damage due to clamping

of the Statimat 4U adapter can be considered very low.

The discrepancy between model and experiments for shorter gauge length ($\leq$ 100 mm) is due to filament waviness and differences in filament lengths. At short yarn lengths, these minor geometrical imperfections become more pronounced and cause non-uniform strain distribution across the yarn. More detailed explanations are given in [67].

4.4 Homogeneous vs. inhomogeneous yarn stress

So far, it has been assumed that a homogeneous stress state in the yarn cross-section increases its overall tensile strength when compared to the counterpart of non-uniformly distributed stress. In this section, we provide a mathematical proof of this intuitive statement.

Let us assume that a bundle of non-interacting parallel brittle fibers is subjected to a global strain ε_{y}, which in the case of the tensile test device equals the clamp displacement u divided by the initial gauge length L:

$$\varepsilon_{\mathrm{y}} = \frac{u}{L}. \tag{4.5}$$

Provided that all fibers are perfectly clamped at the gauge length L, the fiber stress σ_{f} equals $E_{\mathrm{f}}\varepsilon_{\mathrm{y}}$ with E_{f} being the modulus of elasticity of the fibers. During real tensile tests, however, the fibers are not perfectly clamped. Variations in fiber slip in the clamps, initial fiber length and other sources of inhomogeneities can be summarized into an effective modulus of elasticity,$E_{\mathrm{f,eff}}$, which equals

$$E_{\mathrm{f,eff}} = E_{\mathrm{f}} + \epsilon(\varepsilon_{\mathrm{y}}), \tag{4.6}$$

where ϵ is an error term – in general a function of the global yarn strain ε_{y}. Thus, the fiber stress equals

$$\sigma_{\mathrm{f}}(\varepsilon_{\mathrm{y}}) = \varepsilon_{\mathrm{y}} E_{\mathrm{f,eff}} = \varepsilon_{\mathrm{y}}[E_{\mathrm{f}} + \epsilon(\varepsilon_{\mathrm{y}})]. \tag{4.7}$$

The stress of a yarn subjected to ε_{y} is

$$\sigma_{\mathrm{y}}(\varepsilon_{\mathrm{y}}) = \frac{1}{n_{\mathrm{f}}} \sum_{i=1}^{n_{\mathrm{f}}} \sigma_{\mathrm{f},i}(\varepsilon_{\mathrm{y}}), \tag{4.8}$$

where $\sigma_{\mathrm{f},i}(\varepsilon_{\mathrm{y}})$ are stresses in individual fibers corresponding to the global yarn strain. According to [16, 44], the expected fiber stress at any given ε_{y} equals

$$\mathrm{E}[\sigma_{\mathrm{f,i}}(\varepsilon_{\mathrm{y}})] = \varepsilon_{\mathrm{y}} \cdot (E_{\mathrm{f}} + \epsilon_i) \cdot [1 - F(\varepsilon_{\mathrm{y}} \cdot (E_{\mathrm{f}} + \epsilon_i))], \tag{4.9}$$

where $F(\sigma_{\mathrm{f}})$ is the failure probability of a fiber subjected to the stress σ_{f}. If $F(\sigma_{\mathrm{f}})$ is a Weibull distribution with shape m and scale s, the maxima of these expected fibers stresses $\mathrm{E}[\sigma_{\mathrm{f,i}}(\varepsilon_{\mathrm{y}})]$ are given by

$$\mathrm{E}[\sigma_{\mathrm{f,i}}]^{\star} = s \cdot m^{-1/m} \cdot \exp(-1/m) \tag{4.10}$$

and are attained at the strain

$$\varepsilon^{\star}_{\mathrm{f},i} = \frac{s \cdot m^{-1/m}}{E_{\mathrm{f}} + \epsilon_i}, \tag{4.11}$$

which is different for each fiber, see Chapter 2 for derivation of the formulas.

With the substitution of Eq. (4.9), the yarn stress given by Eq. (4.8) becomes (for a large number of fibers)

$$\sigma_{\mathrm{y}}(\varepsilon_{\mathrm{y}}) = \frac{1}{n_{\mathrm{f}}} \sum_{i=1}^{n_{\mathrm{f}}} \mathrm{E}[\sigma_{\mathrm{f,i}}(\varepsilon_{\mathrm{y}})]. \tag{4.12}$$

The maximum of the yarns stress $\sigma^{\star}_{\mathrm{y}}$, i.e. the yarn strength, is attained at the strain $\varepsilon^{\star}_{\mathrm{y}}$:

$$\sigma^{\star}_{\mathrm{y}} = \max[\sigma_{\mathrm{y}}(\varepsilon_{\mathrm{y}})] = \frac{1}{n_{\mathrm{f}}} \sum_{i=1}^{n_{\mathrm{f}}} \mathrm{E}[\sigma_{\mathrm{f,i}}(\varepsilon^{\star}_{\mathrm{y}})]. \tag{4.13}$$

Clearly, Eq. (4.13) is maximized when the global yarn strain equals the fiber strain corresponding to the mean strength of individual filaments, in mathematical form: $\varepsilon^{\star}_{\mathrm{y}} = \varepsilon^{\star}_{\mathrm{f},i}, \forall \varepsilon^{\star}_{\mathrm{f},i}$. This is only possible if the error term ϵ_i in $E_{\mathrm{f,eff}}$ becomes zero, which results in a uniform stress state within the yarn. This gives the proof that uniform stress state results in the maximum possible yarn strength compared to any form of non-uniform stress state.

4.5 Conclusions

The newly developed tensile test device Statimat 4U adapter largely diminishes stress concentrations in high-modulus yarns with brittle filaments and thus measures

higher strengths than other tensile test methods. Both a comparative experiment and theoretical models based on single filament tests confirm the better performance of the new device with a high statistical significance. A combination of the improved testing method for bundles, tests on single filaments and of the fiber bundle model describing the statistical size-effect provides an efficient means for thorough strength characterization of high-modulus multifilament yarns.

Concerning other materials, the positive effect of the adapter clamp could not be observed for aramid, UHMPE and basalt yarns, which have been tested in smaller sample sizes. However, significant differences compared to reference methods were measured for a small sample size of coated carbon yarns (9% polymer matrix). The positive effect of the Statimat 4U adapter on the yarn strength can thus be expected mostly for yarns with very brittle fibers, or generally, fibrous structures prone to local stress concentrations.

5 GLASS FIBER REINFORCED CONCRETE

In this chapter, the behavior of fibrous yarns in composites is demonstrated. In particular, the analyzed composite consists of a cement-based matrix and chopped AR-glass strands which serve as reinforcement for the quasi-brittle matrix. Two approaches to the simulation of the crack bridging effects of chopped AR-glass strands are introduced and compared: a semi-analytical probabilistic model and a discrete rigid body spring network model with semi-discrete representation of the chopped strands. While the probabilistic model has been developed by the author, the latter discrete model has been developed by prof. John E. Bolander from UC Davis and serves merely for reference purposes.

The chopped AR-glass strands exhibit random features at various scales. Fiber strength and interface stress are considered as random variables at the scale of a single fiber bundle while the orientation and position of individual bundles with respect to a crack plane are considered as random variables at the crack bridge scale. At the scale of the whole composite domain, the distribution of fibers and the resulting number of crack-bridging fibers is considered. All these effects contribute to the variability of the crack bridge performance and result in size-dependent behavior of the composite.

The structure of this chapter is as follows: Sec. 5.1 provides an introduction and state of the art report. In Sec. 5.2, a probabilistic approach that predicts statistical moments of the bridging force is described. In Sec. 5.3, a discrete model with semi-discrete representation of the fiber bundles is presented. Both models are compared and their possibilities and limitations are discussed in Sec. 5.5

5.1 Introduction

Glass fibers as reinforcement in cement-based matrix were first utilized in the 1960s in Russia [7]. A further major step towards glass fiber reinforced concrete (GFRC or GRC) is due to the company Owens Corning which developed alkali-resistant (AR) glass by increasing the content (>16%) of zirconia [70, 35] in the material. This

enhancement allowed for the production of a durable high-performance cement-based composite, which has been used in various modifications in structural and military engineering since [5, 52].

Each of the AR-glass fibers is a bundle of (typically 50 to 400) monofilaments which are bonded together by a sizing material. When bridging a crack, these filaments debond and rupture or are being pulled out and thus increase the toughness of the cement-based composite [36]. Moreover, the short dispersed fibers increase the first cracking stress and, above a critical volume fraction threshold, the ultimate tensile strength. These features together with the enhanced durability make the use of GFRC an alternative to traditional steel fiber reinforced concrete (FRC). However, the bridging mechanism is far more complex than in FRC.

Once a crack forms in the matrix, the glass fibers bridging the crack act against further crack opening by stretching and pullout. During this process, some filaments are completely pulled out while others rupture. The mechanism exhibits random features that can be divided into three scales:

1) At the micro scale, individual filaments within a bundle experience random interface shear flow depending on their position within the bundle and thus on the penetration of the matrix into the bundle core. A second source of randomness at the micro scale is the fiber strength that is determined by the weakest flaw in the material structure.
2) At the meso scale, individual bridging fibers are randomly oriented and positioned within the composite domain. This randomness causes variability in the bridging force due to snubbing and non-uniform pullout lengths [34]
3) At the macro scale, the overall number of fibers bridging a crack is a random variable that depends on the specimen geometry, fiber geometry and fiber volume fraction.

A model that considers these sources of random effects and reflects the complexity and unique bridging mechanism of the short glass fiber bundles does not exist to date.

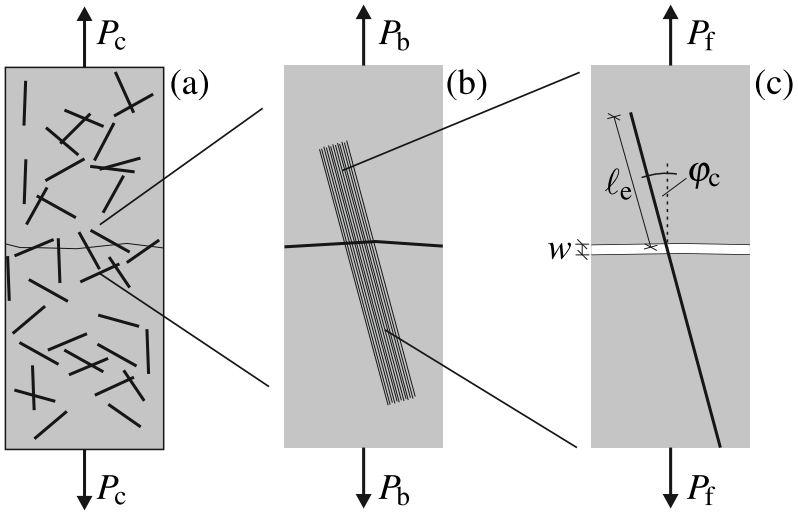

Fig. 5.1: Multiscale approach to the modeling of GFRC: (a) composite crack bridge with multiple filament bundles; (b) filament bundle; (c) single filament considered independently from the bundle.

5.2 Probabilistic model

The semi-analytical probabilistic model is limited to uniaxial tensile loading of a composite with discrete, planar matrix cracks and mechanically independent fibers. The mechanical independence of fibers is provided if matrix deformations are much lower than the fiber deformations i.e. the matrix stiffness $E_\mathrm{m}(1 - V_\mathrm{f}) \gg E_\mathrm{f}V_\mathrm{f}$ is much higher than that of the fibers. Here, E_m and E_f are the matrix and fiber elastic moduli, respectively, and V_f is the fiber volume fraction.

5.2.1 Single filament

Let us assume that the bridging action of a single filament with embedded length ℓ_e and inclination angle φ_c (with respect to the crack plane normal) is provided in the form

$$P_\mathrm{f} = f(w, \ell_\mathrm{e}, \varphi_\mathrm{c}, \boldsymbol{\theta}_\mathrm{r}, \boldsymbol{\theta}_\mathrm{d}), \tag{5.1}$$

where P_f is the bridging force, w is the crack opening, $\boldsymbol{\theta}_\mathrm{d}$ is a vector of deterministic parameters and $\boldsymbol{\theta}_\mathrm{r}$ a vector of random variables defined over the sampling space Ω_r with the corresponding joint distribution function G_{Ω_r}. The mean force transmitted

by a filament within a bundle bridging a matrix crack is

$$\mu_{P_\mathrm{f}}(w, \ell_\mathrm{e}, \varphi_\mathrm{c}) = \mathrm{E}_{\Omega_\mathrm{r}}[P_\mathrm{f}] \tag{5.2}$$

with $\mathrm{E}_\Omega[\mathbf{X}]$ being the expectation operator applied to the random variable $\mathbf{X}$ defined over the sampling space Ω with the joint probability distribution function $G_\Omega(\mathbf{X})$, i.e.

$$\mathrm{E}_\Omega[\mathbf{X}] = \int_\Omega \mathbf{X}\,\mathrm{d}G_\Omega(\mathbf{X}). \tag{5.3}$$

The variance of the filament bridging force is given by

$$\sigma^2_{P_\mathrm{f}}(w, \ell_\mathrm{e}, \varphi_\mathrm{c}) = \mathrm{D}_{\Omega_\mathrm{r}}[P_\mathrm{f}], \tag{5.4}$$

with $\mathrm{D}_\Omega[\mathbf{X}]$ being the variance operator applied to the random variable $\mathbf{X}$ defined over the sampling space Ω with the joint probability distribution function $G_\Omega(\mathbf{X})$, i.e.

$$\mathrm{D}_\Omega[\mathbf{X}] = \mathrm{E}_\Omega[\mathbf{X}^2] - \mathrm{E}_\Omega[\mathbf{X}]^2 = \int_\Omega \mathbf{X}^2\,\mathrm{d}G_\Omega(\mathbf{X}) - \mathrm{E}_\Omega[\mathbf{X}]^2. \tag{5.5}$$

5.2.2 Filament bundle

Given the number of filaments in a bundle, n_f, the force transmitted by the whole bundle reads

$$P_\mathrm{b} = \sum_{i=1}^{n_\mathrm{f}} P_\mathrm{f}(w, \ell_\mathrm{e}, \varphi_\mathrm{c}, \boldsymbol{\theta}_{\mathrm{r},i}, \boldsymbol{\theta}_\mathrm{d}), \tag{5.6}$$

where $\boldsymbol{\theta}_{\mathrm{r},i}$ is the vector of parameters obtained as the i^{th} sample from the sampling space Ω_r of the random variables $\boldsymbol{\theta}_\mathrm{r}$. Since the inclinations and embedded lengths of the bridging bundles will be random, the φ_c and ℓ_e parameters are to be treated as random variables. Their sampling space will be referred to as Ω_φ. The mean bridging force transmitted by a bundle has the form

$$\mu_{P_\mathrm{b}}(w) = \mathrm{E}_{\Omega_\varphi \Omega_\mathrm{r}}[P_\mathrm{b}] = n_\mathrm{f} \mathrm{E}_{\Omega_\varphi \Omega_\mathrm{r}}[P_\mathrm{f}]. \tag{5.7}$$

For the variance of the bundle bridging force, we have to use the law of total variance, which states

$$\mathrm{D}[Y] = \mathrm{E}[\mathrm{D}(Y|X)] + \mathrm{D}[\mathrm{E}(Y|X)]. \tag{5.8}$$

When this law is applied to the present case, $(Y|X)$ is substituted by $P_\mathrm{b}(w, \ell_\mathrm{e}, \varphi_\mathrm{c}, \boldsymbol{\theta}_\mathrm{d}|\boldsymbol{\theta}_\mathrm{r})$. We can alternatively express the conditional probability by explicitly writing the integration domain for individual statistical operators in the equation. With this notation, the variability of the randomly oriented filament bundle with random embedded length reads:

$$\begin{aligned}\sigma^2_{P_\mathrm{b}}(w) &= \mathrm{E}_{\Omega_\phi}\left[\mathrm{D}_{\Omega_\mathrm{r}}(P_\mathrm{b})\right] + \mathrm{D}_{\Omega_\phi}\left[\mathrm{E}_{\Omega_\mathrm{r}}(P_\mathrm{b})\right] \\ &= n_\mathrm{f}^2\left(\mathrm{E}_{\Omega_\phi}[\mathrm{D}_{\Omega_\mathrm{r}}(P_\mathrm{f})] + \mathrm{D}_{\Omega_\phi}[\mathrm{E}_{\Omega_\mathrm{r}}(P_\mathrm{f})]\right).\end{aligned} \tag{5.9}$$

where we do not explicitly write out the dependencies of P_f on its parameters.

5.2.3 Multiple bundles

Let us now introduce the variable n_b, which stands for the number of bundles (chopped strands) bridging a matrix crack. In a composite with randomly dispersed fiber bundles, n_b will be a random variable with sampling space Ω_b. The total force transmitted by all n_b bundles can be written as

$$P_\mathrm{c} = \sum_{j=1}^{n_\mathrm{b}}\sum_{i=1}^{n_\mathrm{f}} P_\mathrm{f}(w, \ell_{\mathrm{e},j}, \varphi_{\mathrm{c},j}, \boldsymbol{\theta}_{\mathrm{r},ij}, \boldsymbol{\theta}_\mathrm{d}) = \sum_{j=1}^{n_\mathrm{b}} P_{\mathrm{b},j}, \tag{5.10}$$

where $\ell_{\mathrm{e},j}$ and $\varphi_{\mathrm{c},j}$ are the j^{th} samples from the Ω_φ sampling space, the vector $\boldsymbol{\theta}_{\mathrm{r},ij}$ is the ij^{th} sample from the sampling space Ω_r and $P_{\mathrm{b},j}$ can be expressed as

$$P_{\mathrm{b},j} = \sum_{i=1}^{n_\mathrm{f}} P_\mathrm{f}(w, \ell_{\mathrm{e},j}, \varphi_{\mathrm{c},j}, \boldsymbol{\theta}_{\mathrm{r},ij}, \boldsymbol{\theta}_\mathrm{d}). \tag{5.11}$$

The mean force resulting from the bridging action of randomly dispersed short fiber bundles has the form

$$\begin{aligned}\mu_{P_\mathrm{c}}(w) &= \mathrm{E}_{\Omega_\mathrm{b}\Omega_\varphi,\Omega_\mathrm{r}}[P_\mathrm{c}] = \mathrm{E}_{\Omega_\mathrm{b}}[n_\mathrm{b}]\,\mu_{P_\mathrm{b}}(w) \\ &= \mathrm{E}_{\Omega_\mathrm{b}}[n_\mathrm{b}]\,n_\mathrm{f}\,\mathrm{E}_{\Omega_\varphi\Omega_\mathrm{r}}[P_\mathrm{f}].\end{aligned} \tag{5.12}$$

Applying the law of total variance according to Eq. (5.8) with $P_\mathrm{c}(w, \ell_\mathrm{e}, \varphi_\mathrm{c}, \boldsymbol{\theta}_\mathrm{r}, \boldsymbol{\theta}_\mathrm{d}|n_\mathrm{b})$ substituted for $(Y|X)$, the variance of the crack bridging force P_c is obtained as

$$\begin{aligned}\sigma^2_{P_\mathrm{c}}(w) &= \mathrm{D}_{\Omega_\mathrm{b}\Omega_\varphi\Omega_\mathrm{r}}[P_\mathrm{c}] = \mathrm{D}_{\Omega_\mathrm{b}\Omega_\varphi\Omega_\mathrm{r}}\left[\sum_{j=1}^{n_\mathrm{b}} P_{\mathrm{b},j}\right] \\ &= \mathrm{E}_{\Omega_\mathrm{b}}\left[\mathrm{D}_{\Omega_\varphi\Omega_\mathrm{r}}\left(\sum_{j=1}^{n_\mathrm{b}} P_{\mathrm{b},j}\,\middle|\, n_\mathrm{b}\right)\right] + \mathrm{D}_{\Omega_\mathrm{b}}\left[\mathrm{E}_{\Omega_\varphi\Omega_\mathrm{r}}\left(\sum_{j=1}^{n_\mathrm{b}} P_{\mathrm{b},j}\,\middle|\, n_\mathrm{b}\right)\right]\end{aligned} \tag{5.13}$$

Exploiting the independence of P_b and n_b, Eq. (5.13) can be simplified to

$$\begin{aligned}\sigma^2_{P_\mathrm{c}}(w) &= \mathrm{E}_{\Omega_\mathrm{b}}\left[n_\mathrm{b}\cdot \mathrm{D}_{\Omega_\varphi\Omega_\mathrm{r}}\left(P_\mathrm{b}\right)\right] + \mathrm{D}_{\Omega_\mathrm{b}}\left[n_\mathrm{b}\cdot \mathrm{E}_{\Omega_\varphi\Omega_\mathrm{r}}\left(P_\mathrm{b}\right)\right] \\ &= \mathrm{E}_{\Omega_\mathrm{b}}[n_\mathrm{b}]\cdot \mathrm{D}_{\Omega_\varphi\Omega_\mathrm{r}}\left[P_\mathrm{b}\right] + \mathrm{D}_{\Omega_\mathrm{b}}[n_\mathrm{b}]\cdot\left(\mathrm{E}_{\Omega_\varphi\Omega_\mathrm{r}}\left[P_\mathrm{b}\right]\right)^2.\end{aligned} \tag{5.14}$$

In order to evaluate the statistical moments of the bridging response, the distribution functions of the random variables need to be known. The derivation of distribution functions for individual random variables is out of the scope of the present publication so that we refer to [56] for the distribution of the strength of a brittle fiber in composite and the bond strength distribution. The distribution of the number of dispersed short fibers bridging a planar matrix crack is in detail dealt with in [65].

5.3 Discrete model

The discrete model developed by John E. Bolander at UC Davis [8] is introduced and used as reference for the probabilistic model described above. In the discrete model, fiber and matrix phase models are both based on a lattice model. The matrix phase is represented by a set of randomly distributed nodes which are interconnected by springs and kinematic constraints. This nodal set for the matrix phase has lattice topology and material properties by the Delaunay/Voronoi tessellations which enable the discretized matrix phase to behave in an elastically homogeneous fashion (Fig. 5.2a). As shown Fig. 5.2b, the matrix element is defined according to the rigid-body-spring concept [8]. The linear and rotational zero-size springs are formed at the centroid C of the area A_{ij} of the Voronoi facet common to nodes i and j. The spring set is constrained to nodes i and j via rigid arm constraints.

The fiber phase can be discretized within the computational domain irrespective of the background lattice representing the matrix [31]. A fiber element is defined wherever a fiber passes through the Voronoi facet A_{ij} associated with a matrix element (Fig. 5.2c). In the semi-discrete fiber model, a linear zero-size spring for the fiber reinforcement is positioned at the intersection point I and aligned with the fiber path. The spring is linked to the associated two nodes i and j through rigid-arm constraints similar to the rigid-body-spring construction of the matrix elements. The semi-discrete modeling of fibers is computationally efficient, contrary

to the fully-discrete fiber modeling in which a fiber is discretized as a series of the frame elements with additional nodal degrees of freedom and its elements are linked to the associated nodes via an ordinary bond link. This feature of the semi-discrete fiber model enables simulations with large numbers of fibers.

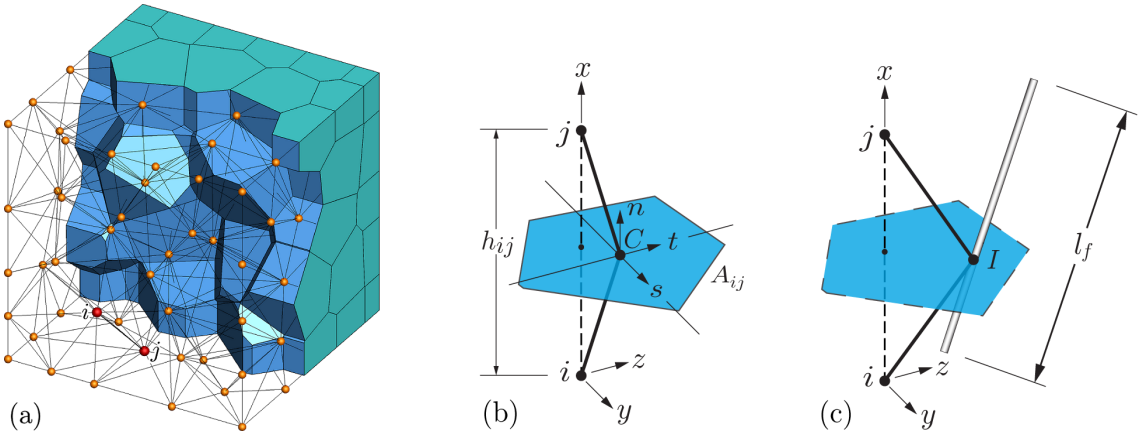

Fig. 5.2: Lattice discretization of fiber reinforced concrete: (a) Delaunay/Voronoi tessellations of material domain; (b) matrix element ij defined by facet centroid C; and (c) fiber element associated with intersection point I.

5.4 Computational example

Having formulated the modeling framework for GFRC in two alternatives, we can proceed to a computational example, which compares the two approaches. Both models require an independent micromechanical model of a fiber bridging action. For this purpose, we apply the analytical form due to [38] with snubbing and spalling effects according to [33]. For reasons of brevity and readability, we simplify the general expressions by assuming a perfectly plastic (frictional) bond with infinite initial stiffness and constant bond strength. With these assumptions, the resulting form for a filament bridging action in the debonding phase reads

$$F_{\mathrm{f,deb}}(w, \sigma_{\mathrm{u}} = \infty) = A_{\mathrm{f}} \sqrt{\frac{2E_{\mathrm{f}}\tau w}{r}} \cdot \exp\left(f\varphi_{\mathrm{c}}\right) \cdot \left(\cos\varphi_{\mathrm{c}}\right)^{s} \tag{5.15}$$

with E_{f}, A_{f} and r being the filament modulus of elasticity, cross-sectional area and radius, respectively, τ denoting the bond strength, f the snubbing coefficient and s

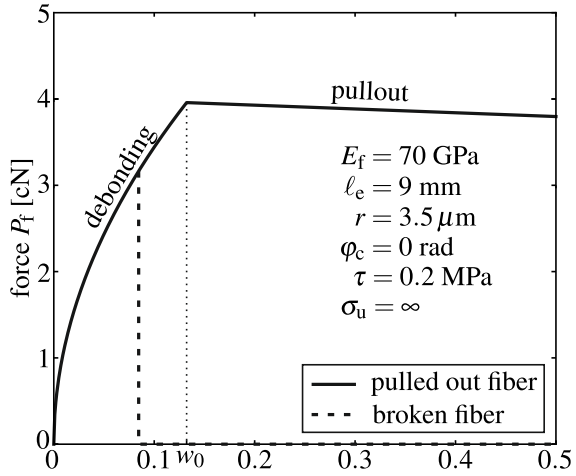

Fig. 5.3: Analytical model of a single fiber bridging action due to Naaman et al. [38].

the spalling coefficient. When the fiber is fully debonded along the embedded length ℓ_e, the pullout stage starts. Again, for reasons of brevity, we ignore any hardening or softening during the pullout stage and write the bridging force during the pullout stage simply as

$$F_{f,pull}(w, \sigma_u = \infty) = 2\pi r\tau(\ell_e + w_0 - w) \cdot \exp(f\varphi_c) \cdot (\cos\varphi_c)^s \tag{5.16}$$

with w_0 being the crack opening at the transition between the debonding and pullout stage. It can be obtained by formulating the continuity condition

$$F_{f,deb}(w_0) = F_{f,pull}(w_0) \rightarrow w_0 = \frac{2\ell_e^2\tau}{rE_f}. \tag{5.17}$$

In both Eq. (5.15) and Eq. (5.16), the assumption was that fibers have an infinite strength $\sigma_u = \infty$. If we now include the possibility of fiber rupture, we have to multiply the fiber force in the debonding phase by $H(\sigma_u - \sigma_f)$, where σ_f denotes the fiber stress and $H(\cdot)$ the Heaviside step function defined as

$$H(x) = \begin{cases} 0 & : x < 0 \\ 1 & : x \geq 0. \end{cases} \tag{5.18}$$

The filament force in the debonding stage then becomes

$$F_{f,deb}(w) = A_f\sqrt{\frac{2E_f\tau w}{r}} \cdot \exp(f\varphi_c) \cdot (\cos\varphi_c)^s \cdot H(\sigma_u - \sigma_f) \tag{5.19}$$

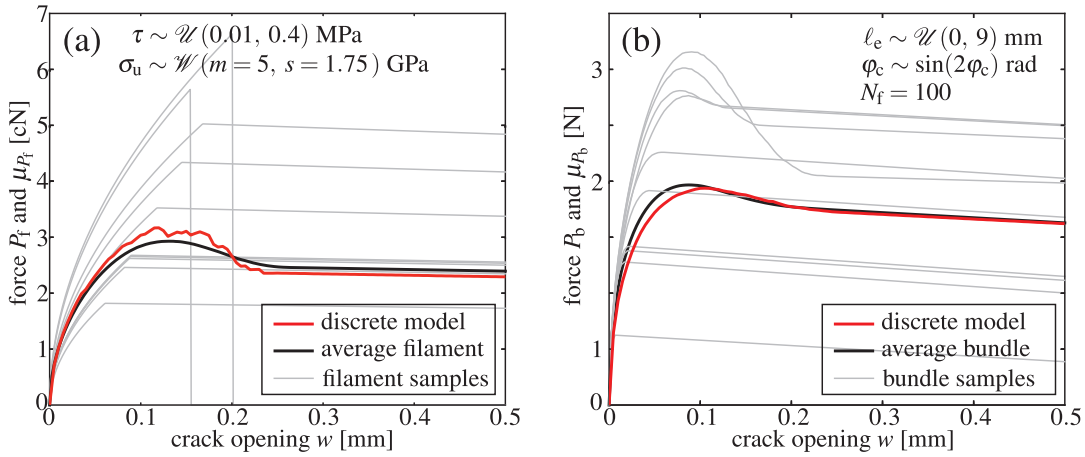

Fig. 5.4: Computational example performed with the present modeling framework: (a) single filament bridging responses (gray curves) sampled from the sampling space of random variables ($\tau \sim$ uniform distribution between 0.01 and 0.4 MPa and $\sigma_u \sim$ Weibull distribution with shape $m = 5$ and scale $s = 1.75$ GPa) and mean filament response (black curve); (b) filament bundle responses sampled from the sampling space of random variables ($\varphi_c \sim \sin(2x)$ distribution and $\ell_e \sim$ uniform distribution between 0 and 9 mm) and mean bundle response (black curve).

with

$$\sigma_f = \frac{F_{f,deb}(w, \sigma_u = \infty)}{A_f}. \tag{5.20}$$

In a similar manner, the pullout force has to be multiplied by a Heaviside function which ensures that fibers have not ruptured at their peak stress during the debonding so that

$$F_{f,pull}(w) = 2\pi r\tau(\ell_e + w_0 - w) \cdot \exp(f\varphi_c) \cdot (\cos\varphi_c)^s \cdot H(\sigma_u - \sigma_{f,max}), \tag{5.21}$$

where

$$\sigma_{f,max} = \frac{2\pi r\tau\ell_e}{A_f}. \tag{5.22}$$

The complete filament bridging action (see Fig. 5.3) can be written as

$$P_f(w) = F_{f,deb}(w) \cdot H(w_0 - w) + F_{f,pull} \cdot H(w - w_0). \tag{5.23}$$

An example of the filament bridging action is depicted in Fig. 5.4a for material parameters that correspond to AR-glass fibers with random τ distributed uniformly

between 0.01 and 0.4 MPa and random fiber strength σ_{u} with Weibull distribution with shape parameter $k = 5$ and scale parameter $\lambda = 1.75$ GPa. The filaments are embedded perpendicular to the crack plane in this example. The figure shows samples from the distributions given by Eq. (5.23) and the mean filament response given by Eq. (5.2), which, multiplied by the number of filaments in a bundle, is the prediction of the response of a perpendicularly embedded filament bundle. The red curve is a single simulation of a bundle consisting of 100 filaments performed by the discrete model.

Fig.5.4b depicts the bridging force of a bundle consisting of $n_{\mathrm{f}} = 100$ filaments with random bond strength and fiber strength as in Fig. 5.4a but, additionally, the orientation angle and embedded length are considered as random variables. Random samples of such filament bundles and the mean bundle bridging force predicted by the probabilistic model with Eq. (5.7) are depicted. The red curve is the bridging force of $n_{\mathrm{b}} = 100$ bundles that are randomly oriented and positioned within the crack predicted by the discrete model.

5.5 Conclusions

Both the probabilistic and the discrete model are capable of simulating the crack bridging action of chopped AR-glass strands in a cement-based matrix. The probabilistic model is computationally very efficient and able to evaluate statistical moments of the response. However, the model formulation includes a number of assumption that make the model of use only for uniaxial tension in its current form.

The discrete model evaluates the response of the composite as a single sample. Therefore, repeated calculations would have to be performed when the variability was of interest. The discrete model, even though more computationally demanding, is much more robust than the probabilistic model. It is not limited to uniaxial tension and is therefore suitable for general purposes. Its comparison with the probabilistic model serves as a verification of the semi-discrete fiber bundle implementation.

SUMMARY

The present thesis proposes probabilistic models of the tensile strength of high-modulus multifilament yarns and glass fiber reinforced concrete. Novel approaches to modeling of the tensile strength of both multifilament yarns and glass fiber reinforced concrete have been derived and described. Regarding the tensile testing of high-modulus multifilament yarns, issues with stress concentrations in clamps of the currently used tensile test machines have been identified. A new clamp device that addresses this issue was developed and validated in comparative experiments with commonly used tensile test machines.

Suggestions for further research

I. multifilament yarns Although the presented work shed light on a variety of aspects of the tensile behavior of high-modulus multifilament yarns, some issues have remained unanswered or have not been answered completely. The following suggestions summarize the open questions and should encourage further research in the field.

In the long run, the approach motivates further work in two directions: First, the industrial testing devices should be enhanced in order to deliver automatic testing of high-modulus multifilament yarns with varied lengths. Second, a more advanced modeling of the mean size effect curve transition between the bundle range and chain-of-bundles range would enable further theoretical conclusions about the re-distribution mechanisms between the filaments within the yarn. In particular, a random-field simulation accounting for effects like position of filaments within the bundle cross-section and the transition from the global to the local load sharing with possibly variable bundle length would provide more insight into the transition from the fiber-bundle to the chain-of-bundles behavior of fibrous yarns.

As the author points out in the corresponding chapter, the transition between the two modes of tensile strength behavior is rather fluent. Especially in the length range between one and two effective bundle lengths, the prediction of the yarn behavior is rather complex. Since this is the length scale of macroscopic structural

elements, the issue surely deserves further attention.

Due to the double-clamp mechanism of the Statimat 4U adapter, it is difficult to measure yarn strain during the tensile test – the reference length changes during the test. This is a severe limitation which has to be addressed if the clamp device is to be released for serial production and used industrially. One possibility is external optical measurement but the device will require a robust built-in solution for strain measurement, eventually.

In course of the validation of the novel clamp device, five materials have been tested. For each material, the parameters of the clamps have to be set in a time consuming procedure. With the design of experiments framework and a software module for the tensile test machine, the optimization of the clamping parameters should be performed automatically with a series of tensile test of the studied material.

A problem that has only been addressed marginally is the tensile testing of coated yarns. Currently used methods are very time consuming and the adapter clamps have proved to yield very good results with this kind of material. In particular, the tensile strengths with coated carbon and basalt yarns were about 9% higher than with standard methods. Taking into account the uprise of coated yarn material, further research in this direction seems to be highly desirable.

II. glass fiber reinforced concrete The probabilistic model derived in Chapter 5 provides a homogenized material model for the tensile response of glass fiber reinforced concrete (GFRC). Its output is a constitutive law, which can be used in the vectorial formulation of microplane responses within the framework of a microplane damage model [58, 59, 57]. With this link to macroscale computation, the probabilistic model is a very useful and computationally convenient means for designing and optimizing GFRC structures.

In order to increase the durability and serviceability of textile reinforced concrete structures, chopped glass fiber bundles are usually added into the cement-based matrix. However, the fiber volume fraction, fiber length and fiber type are parameters that can be easily controlled and modified in order to achieve an optimized struc-

tural behavior under both service loads and in ultimate limit state. An algorithm performing this task requires the model of interaction effects between the bearing textile reinforcement and the toughening chopped fiber reinforcement. This direction should be further investigated if the model is to be applied in structural computation and design.

REFERENCES

[1] A. Abdkader and P. Offermann. Textile Werkstoffe und Flächengebilde zur bautechnischen Verstärkung und Instandsetzung, Teil 1: Deformationskennwerte von AR-Glasfilamenten. *Technische Textilien*, H.4(43):265–266, 268–270, 2000.

[2] A. Abdkader and P. Offermann. Textile Werkstoffe und Flächengebilde zur bautechnischen Verstärkung und Instandsetzung, Teil 3: Deformationskennwerte von AR-Glasfilamenten. *Technische Textilien*, H.1(45):21–23, 2002.

[3] A. Abdkader and P. Offermann. Textile Werkstoffe und Flächengebilde zur bautechnischen Verstärkung und Instandsetzung, Teil 4: Einfluss der Prüfbedingungen und Schlichte auf die Deformationskennwerte von AR-Glasfilamentgarnen. *Technische Textilien*, H.3(45):154–156, 2002.

[4] J. Andersons, R. Joffe, M. Hojo, and S. Ochiai. Glass fibre strength distribution determined by common experimental methods. *Composites Science and Technology*, (62):131–145, 2001.

[5] H. Ball. 35 year review of the grc technology, equipment and markets. In *GRCA Congress*, Istanbul, 2011.

[6] B. Banholzer. *Bond Behaviour of a Multi-filament Yarn Embedded in a Cementitious Matrix*. PhD thesis, 2004.

[7] K.L Biryukovich, Y. Biryukovich, and D.L Biryukovich. *Glass fibre reinforced cement*. CERTA Translation No. 12 Civil Engineering Research Assotiation, London, 1965.

[8] J.E. Bolander and N. Sukumar. Irregular lattice model for quasistatic crack propagation. *Physical Review B*, 71:094106, 2005.

[9] R. Chudoba, M. Vořechovský, V. Eckers, and Th. Gries. Effect of twist, fineness, loading rate and length on tensile bahavior of multifilament yarns (a multivariate study). *Textile Research Journal*, 77(11):880–891, 2007.

[10] R. Chudoba, M. Vořechovský, and M. Konrad. Stochastic modeling of multifilament yarns. I. random properties within the cross-section and size effect. *International Journal of Solids and Structures*, 43(3-4):413–434, 2006.

[11] R. Chudoba, M. Vořechovský, and R. Rypl. Identification of the effective bundle length in a multifilament yarn from the size effect response. *Journal of Composite Materials*, 45(25):2659–2668, 2011.

[12] B. Clauß. Fibers for ceramic matrix composites. In W. Krenkel, editor, *Ceramic Matrix Composites*, pages 1–20. Wiley-VCH Verlag GmbH & Co. KGaA, 2008.

[13] B.D. Coleman. On the strength of classical fibres and fibre bundles. *Journal of Mechanics and Physics of Solids*, 7:60–70, 1958.

[14] T.F. Cooke. Inorganic Fibers-A literature review. *Journal of the American Ceramic Society*, 74(12):2959–2978, 1991.

[15] W.A. Curtin. The tough to brittle transition in brittle matrix composites. *Journal of the Mechanics and Physics of Solids*, 41(2):217–245, 1993.

[16] H.E. Daniels. The statistical theory of the strength of bundles of threads. I. *Proceedings of the Royal Society of London. Series A, Mathematical and Physical Sciences*, 183(995):405–435, 1945.

[17] H.E. Daniels. The maximum of a gaussian process whose mean path has a maximum, with an application to the strength of bundles of fibres. *Advances in Applied Probability*, 21(2):315, Jun 1989.

[18] E. J. Gumbel. *Statistics of Extremes*. Columbia University Press, New York, 1958.

[19] D.G. Harlow and S.L. Phoenix. The chain-of-bundles probability model for the strength of fibrous materials I: Analysis and conjectures. *Journal of Composite Materials*, 12(2):195–214, 1978.

[20] D.G. Harlow and S.L. Phoenix. The chain-of-bundles probability model for the strength of fibrous materials II: a numerical study of convergence. *Journal of Composite Materials*, 12(3):314–334, 1978.

[21] D.G. Harlow and S.L. Phoenix. Probability-distributions for the strength of composite-materials 1. 2 level bounds. *International Journal of Fracture*, 17(4):347–372, 1981.

[22] D.G. Harlow and S.L. Phoenix. Probability-distributions for the strength of composite-materials 2. a convergent sequence of tight bounds. *International Journal of Fracture*, 17(6):601–630, 1981.

[23] D.G. Harlow, R.L. Smith, and H.M. Taylor. Lower tail analysis of the distribution of the strength of load-sharing systems. *Journal of Applied Probability*, 20(2):358–367, 1983.

[24] J.M. Hedgepeth. *Stress concentrations in filamentary structures*. National Aeronautics and Space Administration, 1961.

[25] J.M. Hedgepeth and P.V. Dyke. Local stress concentrations in imperfect filamentary composite materials. *Journal of Composite Materials*, 1(3):294–309, July 1967.

[26] J. Hegger, O. Bruckermann, and S. Voss. AR-Glass and carbon fibers in textile reinforced concrete-simulation and design. *ACI Symposium Publication*, 244-CD:57 – 76, 2007.

[27] J. Hegger, A. Sherif, O. Bruckermann, and M. Konrad. *Textile Reinforced Concrete: Investigations at Different Levels*, volume 224. 2004.

[28] R. Hill and E.U. Okoroafor. Weibull statistics of fibre bundle failure using mechanical and acoustic emission testing: the influence of interfibre friction. *Composites*, 26(10):699–705, 1995.

[29] C.-Y. Hui, S.L. Phoenix, M. Ibnabdeljalil, and R.L. Smith. An exact closed form solution for fragmentation of Weibull fibers in a single filament composite

with applications to fiber-reinforced ceramics. *Journal of the Mechanics and Physics of Solids*, 43(10):1551–1585, 1995.

[30] M. Ibnabdeljalil and W.A. Curtin. Strength and reliability of fiber-reinforced composites: Localized load-sharing and associated size effects. *International Journal of Solids and Structures*, 34(21):2649–2668, 1997.

[31] J. Kang, K. Kim, Y.M. Lim, and J.E. Bolander. Modeling of fiber-reinforced cement composites: Discrete representation of fiber pullout. *International Journal of Solids and Structures*, 51:1970–1979, 2014.

[32] A. Kelly and C. H. Zweben. *Comprehensive Composite Materials: Fiber reinforcements and general theory of composites*. Elsevier, 2000.

[33] Y. Lee, S.T. Kang, and J.K. Kim. Pullout behavior of inclined steel fiber in an ultra-high strength cementitious matrix. *Construction and Building Materials*, 24:2030–2041, 2010.

[34] V.C. Li, Y. Wang, and S. Backer. A micromechanical model of tension-softening and bridging toughening of short random fiber reinforced brittle matrix composites. *Journal of the Mechanics and Physics of Solids*, 39(5):607–625, 1991.

[35] A.J. Majumdar and J.F Ryder. Glass fibre reinforcement for cement products. *Glass Technology*, 9:78–84, 1968.

[36] B. Mobasher and S.P. Shah. Test parameters for evaluating toughness of glass fiber reinforced concrete panels. *Materials Journal*, 86:448–458, 1989.

[37] D.C. Montgomery. *Design and Analysis of Experiments*. John Wiley & Sons, 6. edition edition, December 2004.

[38] A.E. Naaman, G.G. Namur, J.M. Alwan, and H.S. Najm. Fiber pullout and bond slip. I: Analytical study. *Journal of Structural Engineering*, 117(9):2769–2790, 1991.

[39] E.U. Okoroafor and R. Hill. Investigation of complex failure modes in fibre bundles during dynamic mechanical testing using acoustic emission and Weibull

statistics. *Journal of Materials Science Letters*, 30(17):4233–4243, September 1995.

[40] N. Pan. Prediction of statistical strengths of twisted fibre structures. *Journal of Materials Science*, 28(22):6107–6114, 1993.

[41] N. Pan, H. C. Chen, J. Thompson, M. K. Inglesby, S. Khatua, X. S. Zhang, and S. H. Zeronian. The size effects on the mechanical behaviour of fibres. *Journal of Materilas Science*, 10(32):2677–2685, 1997.

[42] N. Pan, H. C. Chen, J. Thompson, M. K. Inglesby, and S. H. Zeronian. Investigation on the strength-size relationship in fibrous structures including composites. *Journal of Materilas Science*, 33:2667–2672, 1998.

[43] Triplicane A. Parthasarathy. Extraction of Weibull Parameters of Fiber Strength from Means and Standard Deviations of Failure Loads and Fiber Diameters. *Journal of the American Ceramic Society*, 84(3):588–592, March 2001.

[44] S.L. Phoenix. Probabilistic strength analysis of fibre bundle structures. *Fibre Science And Technology*, 7:15 – 30, 1974.

[45] S.L. Phoenix, M. Ibnabdeljalil, and C.-Y. Hui. Size effects in the distribution for strength of brittle matrix fibrous composites. *International Journal of Solids and Structures*, 34(5):545–568, February 1997.

[46] S.L. Phoenix and R. Raj. Scalings in fracture probabilities for a brittle matrix fiber composite. *Acta Metallurgica et Materialia*, 40(11):2813–2828, 1992.

[47] S.L. Phoenix and H.M. Taylor. The asymptotic strength distribution of a general fiber bundle. *Advances In Applied Probability*, 5:200 – 216, 1973.

[48] P.K. Porwal, I.J. Beyerlein, and S.L. Phoenix. Statistical strength of twisted fiber bundles with load sharing controlled by frictional length scales. *Journal of Mechanics of Materials and Structures*, 2(4):773–791, 2007.

[49] Rypl R. and R. Chudoba. Multiscale model of the tensile response of brittle matrix composites: Part I probabilistic crack bridge model. *Journal of the Mechanics and Physics of Solids*, 2015. under review.

[50] Rypl R., R. Chudoba, M. Vorechovsky, and X. Li. Multiscale model of the tensile response of brittle matrix composites: Part II probabilistic multiple cracking model and experimental validation. *Journal of the Mechanics and Physics of Solids*, 2015. under review.

[51] M.L. Realff, N. Pang, M. Seo, M.C. Boyce, and S. Backer. A stochastic simulation of the failure process and ultimate strength of blended continuous yarns. *Textile Research Journal*, 70(5):415–430, 2000.

[52] M.J. Roth, C.D. Eamon, T.R. Slawson, T.D. Tonyan, and A. Dubey. Ultra-high-strength, glass fiber-reinforced concrete: Mechanical behavior and numerical modeling. *ACI Materials Journal*, 2:185–194, 2010.

[53] A. Gries Roye and T. Three dimensional and online-shaped textile production with double needle bar raschel machines and weft insertion for concrete applications. *ACI Symposium Publication*, 244-CD:77 – 86, 2007.

[54] R. Rypl. *Probabilistic approach to the mechanics of composites with heterogeneous reinforcement.* PhD thesis, RWTH Aachen University, 2014.

[55] R. Rypl, R. Chudoba, U. Mörschel, S.E. Stapleton, T. Gries, and G. Sommer. A novel tensile test device for effective testing of high-modulus multi-filament yarns. *Journal of Industrial Textiles*, 44(6):934–947, 2015.

[56] R. Rypl, R. Chudoba, A. Scholzen, and M. Vořechovský. Brittle matrix composites with heterogeneous reinforcement: Multi-scale model of a crack bridge with rigid matrix. *Composites Science and Technology*, 89:98–109, December 2013.

[57] A. Scholzen. *Flächige Tragstrukturen aus textilbewehrtem Beton.* PhD thesis, RWTH Aachen University, 2015.

[58] A. Scholzen, R. Chudoba, and J. Hegger. Thin-walled shell structures made of textile-reinforced concrete. *Structural Concrete*, 16(1):106–114, 2015.

[59] A. Scholzen, R. Chudoba, and J. Hegger. Thin-walled shell structures made of textile-reinforced concrete. *Structural Concrete*, 16(1):115–124, 2015.

[60] R.L. Smith. The asymptotic distribution of the strength of a series-parallel system with equal load-sharing. *The Annals of Probability*, 10(1):137–171, 1982.

[61] R.L. Smith and J. C. Naylor. A comparison of maximum likelihood and bayesian estimators for the three- parameter weibull distribution. *Journal of the Royal Statistical Society. Series C (Applied Statistics)*, 36(3):358–369, January 1987. ArticleType: research-article / Full publication date: 1987 / Copyright © 1987 Royal Statistical Society.

[62] R.L. Smith and S.L. Phoenix. Asymptotic distributions for the failure of fibrous materials under series-parallel structure and equal load-sharing. *Journal of Applied Mechanics*, 48:75 – 82, 1981.

[63] Y. Swolfs, L. Gorbatikh, V. Romanov, S. Orlova, S.V. Lomov, and I. Verpoest. Stress concentrations in an impregnated fibre bundle with random fibre packing. *Composites Science and Technology*, 74:113–120, January 2013.

[64] M. Thouless and A. Evans. Effects of pull-out on the mechanical-properties of ceramic-matrix composites. *Acta Metallurgica*, 36(3):517–522, March 1988.

[65] M. Vořechovský, V. Sadílek, and R. Rypl. Probabilistic evaluation of crack bridge performance in fiber reinforced composites. *Engineering mechanics*, 20(1):3–11, 2013.

[66] M. Vořechovský. Incorporation of statistical length scale into weibull strength theory for composites. *Composite Structures*, 92(9):2027–2034, 2010.

[67] M. Vořechovský and R. Chudoba. Stochastic modeling of multifilament yarns: II. random properties over the length and size effect. *International Journal of Solids and Structures*, 43(3-4):435–458, 2006.

[68] A.S. Watson and R.L. Smith. An examination of statistical theories for fibrous materials in the light of experimental data. *Journal of Materials Science*, 20:3260–3270, 1985.

[69] W. Weibull. The phenomenon of rupture in solids. *Royal Swedish Institute of Engineering Research (Ingenioersvetenskaps Akad. Handl.)*, 153:1–55, 1939.

[70] W. Wolf Warren. Glass fiber reinforced cement, 1975. US Patent 3,902,912.

[71] H.F. Wu and A.N. Netravali. Weibull analysis of strength-length relationships in single nicalon SiC fires. *Journal of Materilas Science*, (27):3318–3324, 1992.

[72] H.F. Wu and L.L. Wu. Strength variability and size effect of nicalon fibre bundles. *Journal of Materilas Science*, (29):4232–4237, 1994.

[73] Z. Xia, W.A. Curtin, and T. Okabe. Green's function vs. shear-lag models of damage and failure in fiber composites. *Composites Science and Technology*, 62(10-11):1279–1288, 2002.